

1 **Tracer-based source apportioning of atmospheric organic carbon and**
2 **the influence of anthropogenic emissions on secondary organic aerosol**
3 **formation in Hong Kong**

4 Yubo Cheng¹, Yiqiu Ma^{1,2}, Di Hu^{1,2}

5 ¹State Key Laboratory of Environmental and Biological Analysis, Department of Chemistry, Hong Kong Baptist University,
6 Kowloon Tong, Kowloon, Hong Kong, P. R. China

7 ²HKBU Institute of Research and Continuing Education, Shenzhen Virtual University Park, Shenzhen, 518057, P. R. China

8 *Correspondence to:* Di Hu (dihu@hkbu.edu.hk)

9 **Abstract.** Here we conducted comprehensive chemical characterization and source apportionment of 49 PM_{2.5} samples
10 collected in Hong Kong. Besides the major aerosol constituents, 39 polar organic species, including 14 secondary organic
11 aerosol (SOA) tracers of isoprene, monoterpenes, β -caryophyllene, and naphthalene, were quantified using gas
12 chromatography-mass spectrometry (GC-MS). Six factors, i.e., SOA, secondary sulfate (SS), biomass burning (BB)/SOA, sea
13 salt, marine vessels, and vehicle emissions, were apportioned by positive matrix factorization (PMF) as the major sources of
14 ambient organic carbon (OC) in Hong Kong. The secondary formation, including OC from SOA, SS, and aging of BB plume,
15 was the leading contributor to OC (51.4%, $2.15 \pm 1.37 \mu\text{gC m}^{-3}$) throughout the year. We then applied a tracer-based method
16 (TBM) to estimate the SOA formation from the photo-oxidation of four selected precursors, and monoterpene SOA was the
17 most abundant. A Kintecus kinetic model was used to examine the formation channels of isoprene SOA, and the aerosol-phase
18 ring-opening reaction of isoprene epoxydiols (IEPOX) was found to be the dominant formation pathway. Consistently, IEPOX
19 tracers contributed 94% of total GC-MS quantified isoprene SOA tracers. The TBM-estimated secondary organic carbon
20 (SOC_{TBM}) and PMF-resolved SOC (SOC_{PMF}) showed similar temporal trends; however, SOC_{TBM} only accounted for 26.5% of
21 SOC_{PMF} , indicating a large fraction of ambient SOA was from other reaction pathways/precursors. Results of Pearson's R and
22 multivariate linear regression analysis showed that NO_x processing played a key role in both daytime and nighttime SOA
23 production in the region. Moreover, sulfate had a significant positive linear relationship with SOC_{PMF} and SS-related SOC, and
24 particle acidity was significantly correlated with SOC from the aging of BB.

25 **1 Introduction**

26 Organic aerosol (OA) is a significant component of ambient fine particulate matter (PM_{2.5}). It accounts for 20%-60% of the
27 total PM_{2.5} mass on a global scale (Kanakidou et al., 2005; Van Dingenen et al., 2004; Zhang et al., 2007), and even up to 90%
28 in rural areas (Kanakidou et al., 2005; Roberts et al., 2001; Zhang et al., 2007). OA is either directly emitted into the atmosphere
29 from natural (e.g., vegetative detritus, volcano activity) and anthropogenic sources (e.g., biomass burning (BB), vehicle
30 exhaust, and cooking), or secondarily formed through the oxidation of biogenic and anthropogenic gas-phase precursors and
31 the subsequent partition process or particle-phase reactions (Gelencsér et al., 2007; Hildemann et al., 1996; Hu et al., 2010;
32 Zheng et al., 2014). Given the varying emission sources, meteorological conditions, and anthropogenic activities worldwide
33 and their influences on ambient OA composition, aerosol scientists have put many efforts to investigate the atmospheric
34 processes of OA and their primary and secondary sources, which aid the development of more targeted control policy of PM_{2.5}
35 pollution (Hu et al., 2010; Huang et al., 2014; Schauer et al., 2007; Simoneit, 1999; Stone et al., 2009; Zheng et al., 2005).
36 Huang et al. (2014) applied positive matrix factorization (PMF) to apportion the sources of OA at four urban locations in China,
37 i.e., Beijing, Shanghai, Guangzhou, and Xi'an. They found that secondary formation accounted for a predominant fraction of
38 OA (44-71%) at all four sites. Hong Kong, a megacity located on the southern coast of China in the PRD region and a hub port

39 for the South Asian Pacific region, has its unique OC source characteristics. Hu et al. (2010) incorporated biogenic and
40 anthropogenic SOA tracers and some POA markers into PMF and resolved seven OA sources in Hong Kong. They found that
41 45% of OC in Hong Kong during summertime was from secondary formation, and the number could reach up to 65% on
42 sampling days under regional pollution from the PRD area.

43 All these studies have illustrated the importance of secondary formation to OA in the ambient atmosphere. However, due
44 to SOA's complex chemical composition and formation mechanisms, a precise prediction of SOA load from individual
45 precursors at both regional and global scale is still challenging. An SOA tracer based method (TBM) has been developed to
46 partially solve this problem, which estimates the amount of SOA and SOC formed from the atmospheric oxidation of selected
47 VOCs (i.e., isoprene, monoterpenes, β -caryophyllene, toluene, and naphthalene) using the mass ratios of tracer-to-SOA/SOC
48 obtained from laboratory smog chamber experiments (Kleindienst et al., 2007, 2012). However, TBM can only capture SOC
49 formation from the above-listed VOC precursors, and it may underestimate the actual SOC levels in the ambient atmosphere
50 due to the lack of SOA tracer-to-SOC ratio values of a broader range of OA precursors. Therefore, besides the SOA tracer
51 based method, we have also applied PMF to evaluate the contributions of SOC and primary emissions to OA in the region.

52 Many studies have reported the observational evidence of biogenic SOA enhancement induced by anthropogenic emissions,
53 such as nitrogen oxides (NO_x) and sulfur dioxide (SO_2) (Huang et al., 2014; Xu et al., 2015; Rattanavaraha et al., 2016). NO_x
54 is one of the critical drivers of SOA formation through the photochemical oxidation of VOCs via peroxy radical pathways
55 (Finlayson-Pitts and Pitts, 2000). Nitrogen dioxide (NO_2) reacts with ozone (O_3) to form NO_3 radical, a critical nighttime gas
56 oxidant. Several laboratory studies have reported high SOA yields from the oxidation of biogenic VOCs (BVOCs) by NO_3
57 radical (Fry et al., 2009; Ng et al., 2008). Some field studies also revealed that SOA formation from NO_3 oxidation of BVOCs
58 occurs during both daytime and nighttime (Brown et al., 2013; Rollins et al., 2013). The effect of SO_2 on SOA formation was
59 often explained in the context of particle acidity in laboratory studies, which promotes SOA production through acid-catalyzed
60 heterogeneous reactions (Jang et al., 2002; Surratt et al., 2010). Sulfate was also suggested to enhance isoprene-SOA formation
61 by acting as the nucleophiles, providing active aerosol surface area, and through the salting-in effect (Rattanavaraha et al.,
62 2016; Xu et al., 2015). Recently, Wang et al. (2016) proposed a new sulfate formation pathway in aqueous aerosols through
63 NO_2 oxidation and ammonium neutralization, and synchronous enhancements of both nitrate and SOA production in aqueous
64 aerosols were reported. These laboratory and field monitoring studies have shown that the abundance and chemical nature of
65 ambient OA are significantly influenced by the complex interactions among source emissions, anthropogenic activities,
66 atmospheric physical/chemical processes, and meteorological conditions (An et al., 2019).

67 In this study, we collected 49 $\text{PM}_{2.5}$ samples at an urban site in Hong Kong during a whole year period. Concentration
68 levels of 39 polar organic species were quantified using gas chromatography-mass spectrometry (GC-MS), and their
69 temporal/meteorological variations were evaluated. With the input of SOA tracers and primary source markers into PMF, we

70 quantitatively assessed the contributions of various primary and secondary sources to OC. SOC formed from individual
71 biogenic (i.e., isoprenes, monoterpenes, and β -caryophyllene) and anthropogenic VOCs (i.e., naphthalene) were estimated
72 using the TBM. Finally, the impacts of anthropogenic pollutants (e.g., NO₂, O₃, NO₃, SO₂, and tropospheric odd oxygen (O_x))
73 and PM_{2.5} constituents (e.g., sulfate, acidity, and liquid water content) on total and individual SOCs estimated by both TBM
74 and PMF were evaluated using Pearson's R analysis and multi-linear regression model. This study provides comprehensive
75 information on the sources of OA and SOA in Hong Kong as well as direct evidence of anthropogenic influences on the SOA
76 formation in the region, which may serve as the scientific basis for the formulation of the PM_{2.5} mitigation policy in the region.

77 **2 Method**

78 **2.1. Sample collection**

79 The PM_{2.5} samples were collected on the 12th floor of Science Tower in the Campus of Hong Kong Baptist University
80 (114°15E, 22°13N, ~40 m above the ground), which is a typical urban site. PM_{2.5} samples were collected from September 6,
81 2011, to August 16, 2012, and a total of 49 samples were collected. A high-volume air sampler was used to collect PM_{2.5} onto
82 a quartz fiber filter (20 cm × 25 cm) at a flow rate of 1.13 m³ min⁻¹ for 24 h. The quartz fiber filters were prebaked at 550°C
83 for 24 h to remove organic contaminants. After sampling, the filters were immediately transferred to the laboratory and stored
84 at -18°C until analysis.

85 **2.2. Chemical analysis**

86 For EC and OC analysis, a 1 × 1 cm² filter was cut and analyzed using a thermal and optical transmittance aerosol carbon
87 analyzer (Sunset Laboratory, Tigard, OR, USA). Major ions (i.e., Cl⁻, NO₃⁻, SO₄²⁻, C₂O₄²⁻, Na⁺, Ca²⁺, Mg²⁺, K⁺, NH₄⁺) were
88 identified and quantified by ion-chromatography (IC, DX500, Dionex, Sunnyvale, CA, USA). Vanadium (V) and Nickel (Ni)
89 were analyzed using an Agilent 7900 ICP-MS. Detailed analytical methods for the measurements of EC, OC, and ions were
90 described in our previous work (Hu and Yu, 2013; Ma et al., 2019).

91 Thirty-nine polar organic species were identified and quantified using an Agilent 7890A-5975C GC-MS with prior BSTFA
92 derivatization (N, O-Bis-(trimethylsilyl)trifluoroacetamide, with 1% trimethylchlorosilane, TMCS). For each aerosol sample,
93 20 cm² of the filter was cut into small pieces and sonicated for 10 min with 10 mL of distilled acetonitrile (HPLC grade); the
94 extraction was repeated three times. The extracts were combined and filtered through a Millipore 0.45- μ m PTEE hydrophobic
95 Teflon filter into a 50 mL round flask, concentrated to ~ 0.5 mL by rotary evaporation, and transferred into a 5 mL reaction
96 vial. The round flask was rinsed with 1 mL of acetonitrile for three times, and the rinsing solvent was transferred into the
97 reaction vial as well. The final extract was blown to dryness under a gentle stream of pure nitrogen gas at 40 °C and then
98 derivatized with 100 μ L of BSTFA and 50 μ L of pyridine at 70 °C for 2 h. After the reaction vial cooled down to room

99 temperature, 30 μL of tetracosane- d_{50} (internal standard, 50 $\mu\text{g mL}^{-1}$ in hexane) was added. The derivatives were analyzed by
100 GC-MS. Two microliters of the derivatized sample or standard were injected and separated on an HP-5MS capillary column
101 (30.0m \times 250 $\mu\text{m}\times$ 0.25 μm , Agilent J&W). The temperature program and instrument settings were adapted from the method used
102 by Hu et al. (2008).

103 Saccharides, di- and tricarboxylic acids, 4-nitrocatechol, and cholesterol were identified and quantified using authentic
104 standards. The SOA tracers were identified using surrogate compounds with similar structures and functional groups (Hu et
105 al., 2008; Hu and Yu, 2013), and the detailed information was provided in Table 1. Recovery tests of these organic species
106 were carried out by spiking the mixture of standards onto blank quartz filters, followed by the same sample extraction and
107 analysis processes. Recoveries of the polar compounds were within the range of 80% to 120%. Analysis of hopanes has been
108 reported in our previous study (Ma et al., 2019). Four hopanes, including 17 α ,21 β -hopane, 17 α ,21 β -22R-homhopane,
109 17 α ,21 β -22S-homhopane, and 17 α ,21 β -30-norhopane, were measured using an Agilent 6890N-5975 GC-MS with thermal
110 desorption (TD) method. Recoveries of four hopane standards ranged from 83% to 98%.

111 3 Results

112 Hourly meteorological and air quality data (i.e., temperature, relative humidity (RH), O₃, SO₂, and NO₂) in the vicinity of
113 the sampling site were collected by Hong Kong Environmental Protection Department
114 (HKEPD) (<http://envf.ust.hk/dataview/gts/current/>). During the sampling period, the ambient temperature ranged from 14.52
115 to 31.01 $^{\circ}\text{C}$, with an annual average of 24.17 \pm 5.00 $^{\circ}\text{C}$. The daily average of RH ranged from 52.94% to 97.02%, with a yearly
116 average of 79.87 \pm 10.54%. Heavy rains are common in Hong Kong during summer, which effectively washes out the PM
117 pollutants.

118 Hong Kong is located at the southeast edge of the Pearl River Delta (PRD) region. PRD is a rapidly developing area with
119 intensive industrial activities. As described in our previous studies on the analysis of HULIS and water-soluble PM_{2.5}-induced
120 oxidative potential using the same set of PM_{2.5} samples (Ma et al., 2019; Cheng et al., 2021), we carefully examined the air
121 mass backward trajectories and categorized all sampling days into three groups, i.e., days mainly influenced by the regional
122 pollution from the PRD region (regional days), days influenced by long-regional transport of air mass from the northern and
123 eastern China (LRT days), and days dominated by the locally generated pollutants (local days). The concentration levels of
124 both PM_{2.5} and O₃ and the spatial distribution patterns of SO₂ over the 18 Hong Kong air quality monitoring stations
125 (<http://envf.ust.hk/dataview/gts/current/>) on each sampling day were also checked to assist the classification. A summary of
126 the classification of sampling days and the typical air mass backward-trajectories under the three meteorological categories
127 were presented in Table S2 and Figure S2 in Ma et al. (2019), respectively.

128 The gas pollutants, i.e., O₃, NO₂, O_x, and SO₂, showed significantly higher average concentrations on regional days than

129 those on LRT local days (Table 2). The annual mean concentrations of O₃, NO₂, and SO₂ were 14.85±8.69 ppb, 37.15±9.76
130 ppb, and 4.45±2.57 μg m⁻³, respectively. Given that O₃ and NO₂ undergo a rapid photochemical conversion in the ambient
131 atmosphere, the tropospheric odd oxygen O_X (the sum of O₃ and NO₂) was calculated as an indicator of atmospheric oxidation
132 capacity. As shown in Table 1, O_X ranged from 49.72 to 145.90 μg m⁻³, with a mean value of 99.31±27.42 μg m⁻³, indicating
133 a high oxidation capacity of the Hong Kong atmosphere. The annual average concentrations of OC and EC were 4.18±2.37
134 and 1.02±0.54 μgC m⁻³, respectively. Ambient OC levels observed on regional days (6.15±2.51 μgC m⁻³) were about two times
135 higher than those on LRT and local days; as for EC, it exhibited relative constant levels throughout the year (0.14-2.75 μgC
136 m⁻³). This confirms that EC is mainly emitted locally in Hong Kong, and OC has some regional sources. Moreover, the OC/EC
137 ratios of the collected samples ranged from 1.51 to 10.91, with an annual average value of 4.61, indicating secondary formation
138 could be a dominant source of OA in this region (Mancilla et al., 2015). Our previous study has observed that SOC contributed
139 45% of OC in Hong Kong during the summer of 2006 (Hu et al., 2010). Here the analysis was expanded to samples taken
140 during the 1-yr period to obtain a more comprehensive understanding of sources and their contributions to ambient OA in
141 Hong Kong, and the factors that impact ambient SOA formation.

142 **3.1 Characterization of SOA tracers and other polar oxygenated organic compounds**

143 The concentration levels of 39 organic species, including 14 SOA tracers, 12 saccharides, 11 di- and tricarboxylic acids, 4-
144 nitrocatechol, and cholesterol, under different meteorological conditions, were listed in Table 1.

145 **3.1.1 SOA tracers of isoprene, monoterpenes, β-caryophyllene, and naphthalene**

146 Seven isoprene SOA (Isop_{SOA}) tracers, i.e., 2-methylglyceric acid, two methyltetrol isomers (2-methylthreitol and 2-
147 methylerythritol), three C₅-alkene triol isomers (cis-2-methyl-1,3,4-trihydroxy-1-butene, 3-methyl-2,3,4-trihydroxy-1-butene,
148 and trans-2-methyl-1,3,4-trihydroxy-1-butene), and 3-MeTHF-3,4-diols (including both cis- and trans-3-
149 methyltetrahydrofuran-3,4-diols) were identified and quantified. The sum of all Isop_{SOA} tracers ranged from 1.67 to 117.17
150 ng m⁻³, with the annual mean value of 22.78±26.06 ng m⁻³. Among the Isop_{SOA} tracers, methyltetrols and C₅-alkene triols
151 were the most abundant, and they are suggested to be formed through the acid-catalyzed ring-opening reactions of IEPOX
152 under low-NO_X condition (Chan et al., 2010; Surratt et al., 2010). Higher concentrations of Isop_{SOA} tracers were measured in
153 summer and autumn than in winter and spring. This could be caused by the higher temperature, stronger solar radiation, and
154 higher emission of isoprene in summer and autumn than in the other two seasons, which promoted the SOA formation from
155 isoprene. This seasonal pattern is consistent with what were observed in other studies (Ding et al., 2012; Kleindienst et al.,
156 2007; Lewandowski et al., 2008). However, if we compare the levels of isoprene tracers monitored at different sites during
157 summer, the total amount of Isop_{SOA} tracers measured in Hong Kong was about five times lower than those measured in

158 several cities in the U.S. and a rural site (WQS site) in the PRD area (Ding et al., 2012; Kleindienst et al., 2007; Lewandowski
159 et al., 2008). This may be due to the different levels of isoprene, OH radical, and NO_x at these sampling sites. The 3-MeTHF-
160 3,4-diols, tracers formed through the intermolecular rearrangement of isoprene epoxydiols (IEPOX) under acidic conditions,
161 was identified in Hong Kong PM_{2.5} samples for the first time. It has an annual mean concentration of 0.23±0.10 ng m⁻³, which
162 was about 70 times lower than that in Birmingham, U.S. (Rattanavaraha et al., 2016), but was comparable to what was observed
163 at the WQS site in the PRD area (He et al., 2018). 2-Methylglyceric acid, an isoprene tracer formed from methacrylic acid
164 epoxide (MAE) and hydroxymethyl-methyl- α -lactone (HMML) under high-NO_x conditions (Lin et al., 2013; Nguyen et al.,
165 2015), presented a quite different temporal trend from those of the other six Isop_{SOA} tracers, with the highest concentration in
166 winter, and then autumn, summer, and spring. Chamber studies suggested that MAE is an oxidation product resulting from the
167 OH addition to methacryloylperoxynitrate (MPAN) and its production is temperature dependent (Roberts and Bertman, 1992;
168 Worton et al., 2013). Under higher temperatures, the loss of MPAN is dominated by thermal decomposition, which does not
169 produce SOA tracers through the NO/NO₂ pathway. Under lower temperature, thermal decomposition of MPAN is limited and
170 more MPAN reacts with OH to generate MAE. Therefore, the lower temperatures in winter would favor the production of
171 MAE and the MAE Isop_{SOA} tracers, such as 2-methylglyceric acid. Moreover, all Isop_{SOA} tracers exhibited higher
172 concentrations on regional days than LRT and local days. On regional days, air masses transported from the PRD area worsened
173 the air quality in Hong Kong, and the higher levels of gaseous pollutants, e.g., O₃, NO₂, O_x, and SO₂ (Table 2), promoted SOA
174 formation.

175 Generally speaking, at an urban location with anthropogenic NO_x emissions from automobiles and power plants, the
176 generation of Isop_{SOA} tracers from the MAE NO/NO₂ pathway should be more favored than the IEPOX HO₂ channel.
177 However, in this study, 94% of the total mass of the quantified Isop_{SOA} tracers were produced through the IEPOX HO₂
178 pathway. A similar phenomenon was observed at the WQS site in the PRD region (He et al., 2018). Therefore, to better
179 understand the influences of environmental factors on isoprene SOA formation in the region, we applied the kinetic models
180 described by Eddingsaas et al. (2010), Worton et al. (2013), and Birdsall et al. (2014) to investigate the fate of both IEPOX
181 and MAE in the atmosphere. Besides their degradation through acid-catalyzed ring-opening reactions on particles, IEPOX and
182 MAE can also be oxidized in the gas phase or removed by dry deposition (Eddingsaas et al., 2010). We applied the Kintecus
183 kinetic model (Ianni, 2015) to quantitatively evaluate the fractions of these two Isop_{SOA} intermediates that undergo gas-
184 phase oxidation, aerosol-phase acid-catalyzed ring-opening reaction, and dry deposition processes. Details of the model
185 calculations were provided in the appendices.

186 Figure 1 showed the comparison of the three elimination processes of IEPOX and MAE during the sampling period in
187 Hong Kong. Given the high volatility of MAE (vapor pressure: 9.2×10^{-5} atm) (Worton et al., 2013), it has a low tendency to
188 partition onto the particle phase and its uptake onto aqueous particles is mainly governed by Henry's law constant (k_H^{cp}).

189 Worton et al. (2013) estimated the $k_{\text{H}^{\text{CP}}}$ value of MAE to be $7.5 \times 10^6 \text{ M atm}^{-1}$, which is 20 times lower than that of IEPOX
190 ($1.3 \times 10^8 \text{ M atm}^{-1}$). Moreover, Riedel et al. (2015) suggested that the heterogeneous reactive uptake coefficient of MAE ($\gamma =$
191 4.9×10^{-4}) through the ring-opening reaction was a factor of 30 lower than that of IEPOX. Therefore, as shown in Fig. 1, MAE
192 was primarily eliminated by dry deposition ($> 80\%$) in the gas phase, and only a trivial fraction was degraded through the ring-
193 opening reactions ($\leq 2\%$). Our results on the fate of MAE were similar to those observed at the University of California-
194 Blodgett Forest Research Station (UC-BFRS) (Worton et al., 2013). However, our results on the relative contributions of these
195 three degradation pathways to IEPOX loss were quite different from theirs, indicating a more sensitive response of IEPOX
196 than MAE to the change of environmental oxidants and conditions. Given the high liquid water content (LWC; mean:
197 $57.20 \pm 37.15 \mu\text{g m}^{-3}$) and particle acidity (H_p^+ ; mean: -0.28 ± 0.42) of $\text{PM}_{2.5}$ samples in this study (Table 2), particle-phase ring-
198 opening reaction (F_{rop}) was the dominant degradation pathway of IEPOX in the Hong Kong atmosphere (average: 97.6%), and
199 its loss through dry deposition and gas-phase oxidation is almost negligible. The F_{rop} of IEPOX reported by Worton et al. (2013)
200 was only 0.02%, mainly due to the much lower LWC (mean: $0.4 \mu\text{g m}^{-3}$) and weaker H_p^+ (pH mean: 4.4) of their $\text{PM}_{2.5}$ samples.
201 These results demonstrated that particle-phase LWC and H_p^+ played a more significant role in the atmospheric degradation of
202 IEPOX than MAE. Results from the kinetic model simulation were strongly supported by the experimental finding of IEPOX
203 tracers as the dominant Isop_{SOA} tracers measured in Hong Kong. The average ratio of IEPOX tracers to MAE tracers was
204 16.54 (ranged from 3.00 to 71.58), and the average value of $F_{\text{rop-IEPOX}}/F_{\text{rop-MAE}}$ was 191.92, confirming that the IEPOX HO_2
205 channel is the major formation pathway of isoprene SOA in the region.

206 Five SOA tracers of monoterpenes (Mono_{SOA}), i.e., 3-hydroxyglutaric acid, 3-hydroxy-4,4-dimethylglutaric acid, 3-
207 methyl-1,2,3-butanetricarboxylic acid, 3-isopropylpentanedioic acid, and 3-acetyl pentanedioic acid, were identified and
208 quantified. Their summed concentrations ranged from 2.54 to 32.57 ng m^{-3} , with an annual average value of $10.76 \pm 8.04 \text{ ng m}^{-3}$,
209 comparable to that reported at the WQS site in the PRD region but lower than that measured in the U.S. (Ding et al., 2012;
210 Kleindienst et al., 2007; Lewandowski et al., 2008). All Mono_{SOA} tracers showed the highest level on regional days (mean:
211 $18.00 \pm 9.28 \text{ ng m}^{-3}$), followed by LRT (mean: $10.31 \pm 7.33 \text{ ng m}^{-3}$) and local days (mean: $6.41 \pm 2.75 \text{ ng m}^{-3}$) (Table 1). Although
212 a higher emission and faster photochemical degradation of monoterpenes are expected in summer due to the intense solar
213 radiation and high temperature, higher levels of Mono_{SOA} tracers were monitored in autumn and winter than in the other two
214 seasons, similar to what observed at the WQS site (Ding et al., 2014). This seasonal trend of monoterpene SOA tracers may
215 be partly due to the lower mixing height and temperature during autumn/winter, which favored the partition of Mono_{SOA}
216 tracers onto the aerosol phase. Moreover, most of the regional days were identified in autumn and winter. The higher levels of
217 NO_x , O_3 , O_x , and SO_2 on regional days (Table 2) are also responsible for the enhanced monoterpene SOA production in autumn
218 and winter. Among Mono_{SOA} tracers, 3-hydroxyglutaric acid (3HGA) was the most abundant, contributing $\sim 60\%$ of the total
219 mass of Mono_{SOA} tracers. Smog chamber experiments showed that the production yield of 3-methyl-1,2,3-butanetricarboxylic

220 acid (MBTCA) from α -pinene/NO_x oxidation was significantly higher than those from the β -pinene/NO_x and d-limonene/NO_x
221 experiments (Jaoui et al., 2005). Therefore, the ratio of 3HGA/MBTCA was used as a criterion to differentiate SOA from α -
222 pinene and other monoterpenes (Ding et al., 2014). The value of this ratio was obviously higher on regional days (8.58±2.69)
223 than those on LRT (6.64±3.63) and local days (5.62±3.14), indicating that monoterpenes other than α -pinene, such as β -pinene
224 and d-limonene, might have a more significant contribution to SOA on regional days in the region.

225 *beta*-Caryophyllinic acid is the SOA (Cary_{SOA}) tracer of β -caryophyllene, and it ranged from 0.49 to 5.82 ng m⁻³, with
226 an average annual mean value of 1.53±1.07 ng m⁻³. Similar to the other SOA tracers, β -caryophyllinic acid showed the highest
227 concentrations on regional days (mean: 2.33±1.21 ng m⁻³) than LRT (1.73±1.16 ng m⁻³) and local days (0.94±0.41 ng m⁻³)
228 (Table 1). For its seasonal trend, β -caryophyllinic acid also exhibited the highest concentration in autumn and winter than the
229 other two seasons. The SOA tracer of toluene, 2,3-dihydroxy-4-oxopentanoic acid, was undetectable in this study, mainly due
230 to its trace level in the Hong Kong atmosphere (Hu et al., 2008) and the limited sensitivity of GC-quadrupole MS. Even in our
231 previous study on a batch of summer PM_{2.5} samples using a more sensitive GC-ion trap MS, it was barely quantified with a
232 concentration of less than 1 ng m⁻³ in most samples (Hu et al., 2008). Phthalic acid was suggested as the SOA tracer of
233 naphthalene, given its abundance in both naphthalene-SOA and ambient OA (Kleindienst et al., 2012). With the awareness of
234 the potential uncertainties, e.g., the primary origin of phthalic acid from biomass burning, we adopted phthalic acid as the SOA
235 tracer of naphthalene representing the SOA formation from anthropogenic VOCs. The concentration levels of phthalic acid
236 ranged from 0.80 to 16.42 ng m⁻³, with an average of 4.31±3.39 ng m⁻³. Similar to the other SOA tracers, it also showed the
237 highest concentrations on regional days (7.16±3.61 ng m⁻³) than LRT (4.97±3.30 ng m⁻³) and local days (2.26±1.38 ng m⁻³)
238 (Table 1).

239 3.1.2 Saccharides and dicarboxylic acids

240 Twelve saccharides, i.e., levoglucosan, arabinol, fructose, meso-erythritol, sucrose, galactosan, mannitol, sorbitol,
241 galactose, glucose, xylose, and xylitol, have been quantified. Of the 12 saccharides, levoglucosan, the tracer of BB, was by far
242 the most abundant (range: 0.64-474.15 ng m⁻³; mean: 75.02±111.43 ng m⁻³). It showed the highest levels on regional days
243 (about 6 times higher than that on local days), especially during winter when BB activities in the PRD region were most
244 frequent. Two primary saccharides, i.e., fructose and xylose, also exhibited the highest levels on regional days. They showed
245 good correlations with levoglucosan ($R^2= 0.65$ and 0.93), suggesting that they could be from BB as well.

246 Among the identified dicarboxylic acids, oxalic acid was the most abundant, followed by terephthalic acid, phthalic acid,
247 malic acid, succinic acid, and others. Most dicarboxylic acids, including the five most abundant ones, showed higher levels on
248 regional days; they were found with higher levels in winter and autumn as well. This temporal trend is similar to what we have
249 observed for Mono_{SOA} tracers and most saccharides, indicating that regional pollution had a dominant influence on the

250 abundance of both primary and secondary aerosols in Hong Kong, far exceeding the influence of other environmental
251 parameters, such as temperature and solar radiation. Atmospheric dicarboxylic acids have various sources. For example, oxalic
252 acid was suggested to be secondarily formed from biogenic emissions and anthropogenic sources (e.g., BB and automobile
253 exhaust) through both gas-phase reactions and in-cloud processing (Yu et al., 2005). Malic acid was suggested to be the photo-
254 degradation product of both succinic acid and biogenic SOA compounds (Hu and Yu, 2013). In this study, malic acid was
255 found to be strongly correlated with 3HGA ($R^2=0.96$) and Σ Mono_{SOA} tracers ($R^2=0.95$) throughout the year, providing more
256 evidence to the hypothesis that malic acid is a late-stage oxidation product of BVOCs, especially monoterpenes (Hu and Yu,
257 2013). Ambient terephthalic acid was mainly directly emitted from plastic wastes incineration (Simoneit et al., 2005) and was
258 used as a marker of waste incineration.

259 Besides dicarboxylic acids, two benzenetricarboxylic acids (i.e., 1,2,3- and 1,2,4-benzenetricarboxylic acids), 4-
260 nitrocatechol, and cholesterol were also quantified. The two benzenetricarboxylic acids were suggested to be the photo-
261 degradation products of polycyclic aromatic hydrocarbons (PAHs) emitted from the combustion activities (Kautzman et al.,
262 2010). We have previously identified them in the water-soluble humic-like substances (HULIS) extracts of PM_{2.5} samples
263 collected in Beijing and Hong Kong (Ma et al., 2018, 2019). The annual mean concentrations of 1,2,3- and 1,2,4-
264 benzenetricarboxylic acids measured in this study were 2.27 ± 1.97 ng m⁻³ (range: 0.47-9.50 ng m⁻³) and 3.13 ± 2.68 ng m⁻³ (0.47-
265 12.54 ng m⁻³), respectively, which were comparable to what measured at the other four sites in the PRD region (He et al., 2018).
266 The 4-nitrocatechol, which was secondarily generated from the photo-oxidation of naphthalene, was suggested as the tracer of
267 atmospheric aging of BB plume (Kitanovski et al., 2012). It strongly correlated with levoglucosan ($R^2=0.88$) and exhibited
268 higher levels on regional days and during winter, which further confirmed its BB origin in the region. Therefore, the two
269 benzenetricarboxylic acids and 4-nitrocatechol were included in PMF analysis as the SOA tracers of BB aging.

270 3.2 Source apportionment of organic aerosols

271 In this study, the US EPA PMF 5.0 was used to determine the major OA sources and quantify their contributions to OC.
272 Eighteen species were input into PMF, including EC, OC, Ni, V, major ions, and various primary and secondary organic tracers.
273 Given their similar origins, some organic tracers were lumped together, and the lumped species were used as the fitting species
274 in PMF. They were (1) C₅-alkene triols, sum of the three C₅-alkene triols isomers; (2) IsopT, the sum of two methyltetrol
275 isomers and 2-methyl glyceric acid; (3) MonoT, the sum of the five monoterpenes SOA tracers; and (4) Hopane, the sum of
276 the four hopanes. Since C₅-alkene triols were not in the SOA tracers list of the TBM (Kleindienst et al., 2007), the lumped C₅-
277 alkene triols were used as a separated fitting species in PMF. PMF solutions were tested with 4 to 8 factors. A hundred base
278 runs were performed in each modeling run, and the run with the minimum Q value was selected. The uncertainty values of
279 each input species were calculated using the method described in our previous studies (Hu et al., 2010; Ma et al., 2016), which

280 were set to be 20% of the mean concentrations for OC and EC, and 40% of mean values for cations, anions, and all organic
 281 species. An extra modeling uncertainty of 10% was used to account for possible temporal changes in the source profiles. The
 282 $Q_{\text{Robust}}/Q_{\text{True}}$ ratio was 1.00, and scaled residuals were normally distributed between -0.2 and 0.2, indicating no influence of
 283 outliers on the solution. A hundred bootstrap runs were performed with a minimum correlation R-value to examine the base
 284 run solution's stability and uncertainty. All bootstrapped factors were explicitly mapped to factors resolved in base solution
 285 with no exception. In the displacement (DISP) assessment, no error was found, and the drop of Q value was less than 1%,
 286 suggesting a stable solution. No swap factor appeared at $dQ_{\text{max}}=4$, indicating there was no considerable rotational ambiguity
 287 in the solution. Rotations were introduced to the solutions by adjusting the FPEAK value from -1 to +1, and the non-rotated
 288 solutions (FPEAK=0.0) were considered to be the most interpretable ones. Moreover, a strong linear correlation between the
 289 measured and PMF-predicted OC (OC_{PMF}) ($R^2=0.92$) was observed, which also suggested a reliable PMF solution.

290 As shown in Fig. 2, the first factor was distinguished by high loadings of oxalate and biogenic SOA tracers, suggesting
 291 the secondary origin of this source. The second factor was dominated by large amounts of SO_4^{2-} and NH_4^+ , suggesting the
 292 process of secondary sulfate formation. In the third factor, about 90% of levoglucosan was resolved into it, accompanied by
 293 4-nitrocatechol, phthalic acid, and the two benzenetricarboxylic acids, indicating both the primary emission and aging of BB
 294 plume. Therefore, this factor was defined as BB and SOA (BB/SOA). The fourth factor was identified as vehicular emissions
 295 due to the large amounts of hopanes and EC resolved. The fifth factor has large amounts of Ni and V, which are signatures of
 296 residual oil combustion from the marine vessel (Viana et al., 2009). It is well known that Hong Kong is one of the busiest
 297 container ports globally, which handles 50% of the PRD's total cargo throughput. Therefore, the fifth factor was identified as
 298 marine vessels. The sixth factor has a high loading of Na^+ , Mg^{2+} , and Ca^{2+} , indicating the sea salt source.

299 The amount of OC apportioned to each factor in PMF analysis was considered as the contribution of that source to ambient
 300 OC. Therefore, the two leading sources contributing to ambient OC in Hong Kong were BB (including both primary emission
 301 and aging process, OC_{BB} : 27.9%, $1.17\pm 1.99 \mu\text{gC m}^{-3}$) and SOA (SOC_{SOA} : 27.5%, $1.15\pm 0.82 \mu\text{gC m}^{-3}$), followed by marine
 302 vessels (OC_{marine} : 15.6%, $0.65\pm 0.58 \mu\text{gC m}^{-3}$), SS (SOC_{SS} : 14.5%, $0.60\pm 0.46 \mu\text{gC m}^{-3}$), vehicle emissions (OC_{vehicle} : 10.5%,
 303 $0.44\pm 0.42 \mu\text{gC m}^{-3}$), and sea salt (OC_{sea} : 4.0%, $0.17\pm 0.19 \mu\text{gC m}^{-3}$) (Table 2 and Fig. 3). Since a fraction of SOA from the
 304 aging of BB (SOC_{BB}) was resolved into the BB/SOA factor, we calculated SOC_{BB} using the following equation:

$$305 \quad SOC_{\text{BB}} = OC_{\text{BB}} - \frac{[LEVO_{\text{BB}}]}{0.082} \quad (1)$$

306 where OC_{BB} and $[LEVO_{\text{BB}}]$ are the amounts of OC and levoglucosan resolved in the BB/SOA factor. Using levoglucosan
 307 as the tracer of primarily emitted BB OA, we calculated the amounts of POC from BB (POC_{BB}) by dividing $[LEVO]_{\text{BB}}$ with
 308 0.082, where 0.082 is the average ratio of levoglucosan to POC from the burning of major types of Chinese cereal straws (i.e.,
 309 rice, wheat, and corn) obtained in the combustion chamber experiments (Zhang et al., 2007). As cereal straws are one of the
 310 most common BB fuels in China, the above ratio (0.082) has been used to estimate BB contribution to POC in both Beijing

311 (Zhang et al., 2008) and Hong Kong (Sang et al., 2011). Therefore, it was adopted to calculate POC_{BB} in this study.

312 Based on PMF results, the source-specific contributions to OC were presented in Table 2 and demonstrated in Fig. 3. The
313 total SOC apportioned by PMF (SOC_{PMF}), i.e., the sum of SOC_{SOA} , SOC_{SS} , and SOC_{BB} , accounted for 51.4% ($2.15 \pm 1.37 \mu\text{gC}$
314 m^{-3}) of OC in Hong Kong, with the secondary organic-rich sources (i.e., $SOC_{SOA} + SOC_{BB}$) contributing 36.9% ($1.54 \pm 1.13 \mu\text{gC}$
315 m^{-3}) of total OC. Huang et al. (2014) also reported that secondary organic-rich sources accounted for 30-40% of OC in
316 Guangzhou, another PRD site. A higher level of SOC_{PMF} and its contribution to OC were observed on regional days (3.27 ± 1.18
317 $\mu\text{gC m}^{-3}$, 57.4%) than on LRT ($2.36 \pm 1.54 \mu\text{gC m}^{-3}$, 53.0%) and local days ($1.36 \pm 0.81 \mu\text{gC m}^{-3}$, 43.6%). An even starker
318 difference in the amounts of SOC_{BB} between regional and local days was observed, which was eight times higher on the
319 regional days. This suggested that non-local sources were the dominant contributors to SOC_{BB} . BB activities were intensive in
320 the PRD region, especially during fall and winter. On regional days, freshly emitted and aged gaseous and aerosol phase
321 pollutants from the open burning of rice straws and other crops were transported from the northern PRD region into Hong
322 Kong (Hu et al., 2010). Huang et al. (2014) examined the aging of BB plume at low temperatures. They found that the
323 production of BB SOA was rapid at a typical OH radical concentration of wintertime China, and the amount of BB SOA may
324 exceed BB POA in 4-14 h even at -10°C . Given that the average temperature in Hong Kong during autumn and winter was
325 26.15°C and 17.76°C , the formation of BB SOA should be even fastly achieved during the regional transport. As expected,
326 SOC_{SOA} also showed a higher average concentration on regional days ($1.75 \pm 0.75 \mu\text{gC m}^{-3}$) than on LRT ($1.14 \pm 0.82 \mu\text{gC m}^{-3}$)
327 and local days ($0.78 \pm 0.65 \mu\text{gC m}^{-3}$), which is consistent with the trends of all SOA tracers. Although SOC from secondary
328 inorganic-rich source (SOC_{SS}) exhibited the highest levels ($0.82 \pm 0.38 \mu\text{gC m}^{-3}$) on regional days as well, its contribution to
329 OC was relatively stable under the three synoptic conditions (Fig. 3). Several studies showed that SO_2 transported from the
330 northern PRD region promoted secondary sulfate formation in Hong Kong through both gas-phase and in-cloud oxidation
331 pathways (Lu and Fung, 2016; Yu et al., 2005; Yuan et al., 2006). A recent study proposed that the sulfate formation in aqueous
332 aerosols through NO_2 oxidation and ammonium neutralization can simultaneously enhance the production of both nitrate and
333 SOA (Wang et al., 2016), which helps explain the considerable amount of SOC_{SS} apportioned.

334 OC from the four primary sources, i.e., POC_{BB} , OC_{marine} , OC_{vehicle} , and OC_{sea} , accounted for 48.6% of total OC throughout
335 the year. Similar to SOC_{BB} , POC_{BB} showed a higher level ($1.38 \pm 1.75 \mu\text{gC m}^{-3}$) on regional days due to a large number of
336 emissions from BB activities in the northern PRD area. OC_{vehicle} remained a higher contribution on local days (15.6%,
337 $0.49 \pm 0.46 \mu\text{gC m}^{-3}$), consistent with our previous finding that vehicle emission is a local pollution source (Hu et al., 2010).
338 Similarly, marine vessels accounted for a greater amount and larger fraction of OC on local days (32.0%, $1.00 \pm 0.63 \mu\text{gC m}^{-3}$)
339 than LRT (5.2%, $0.23 \pm 0.19 \mu\text{gC m}^{-3}$) and regional days (6.5%, $0.37 \pm 0.21 \mu\text{gC m}^{-3}$). On local days, the southeastern to
340 southwestern wind brought pollutants from residual oil combustion from the ocean into Hong Kong, leading to a higher
341 OC_{marine} .

342 In summary, both secondary aerosol sources and air mass origins play important roles in atmospheric OC in Hong Kong.
343 On regional days, air mass transported from the northern PRD area brought large amounts of air pollutants into Hong Kong,
344 which promoted the SOA production from both anthropogenic emissions and BVOCs and resulted in a fraction of 57.4% of
345 OC being secondarily formed. On the other hand, local sources, including vehicle emissions and marine vessels, became more
346 critical and significantly contributed to OC (56.4%) on local days.

347 3.3 Estimation of SOC origin

348 To better understand the SOA precursors and their contributions to SOA/SOC in the region, we adopted a tracer-based
349 method (Kleindienst et al., 2007, 2012; Offenberg et al., 2007) to estimate the SOA/SOC formation from a group of selected
350 biogenic and anthropogenic hydrocarbons, i.e., isoprene, monoterpenes, β -caryophyllene, and naphthalene. The mass ratio of
351 tracer compounds to the total SOC (f_{SOC}) generated from individual VOC precursors was derived from smog chamber
352 experiments (Kleindienst et al., 2007; Offenberg et al., 2007). By assuming the same f_{SOC} value of the precursor under smog
353 chamber conditions and in ambient air, one can use the quantified SOA tracer concentrations to estimate the amount of SOC
354 from that precursor in the real atmosphere. It has been well noted that results obtained from this tracer-based method are subject
355 to potential uncertainties from various aspects, e.g., the larger variation of precursor concentrations and more complicated
356 environmental conditions in the real atmosphere than in smog chamber experiments, the decay of some tracer compounds
357 during transport, mismatch of ambient and smog chamber generated SOA compositions, using surrogates other than ketopinic
358 acid for the quantification of tracer compounds, and so on (Ding et al., 2014; Hu et al., 2008; Kleindienst et al., 2012, 2007).
359 However, using the tracer-based method, we can at least have a rough estimation of the key SOA precursors in the region,
360 their contributions to ambient OC, and the amount of SOC from unknown precursors. Wang et al. (2013) noted that the SOA
361 tracer-based method would significantly underestimate SOC_{Mono} in the PRD region. Ding et al. (2014) gave a reasonable
362 explanation that the mismatch of monoterpene tracers measured in ambient air and used to derive f_{SOC} of monoterpenes in
363 chamber studies may increase the uncertainty of SOC_{Mono} . Thus they picked the five Mono_{SOA} tracers measured in their
364 samples and derived the f_{SOC} and f_{SOA} values using the SOA tracers data and SOA/SOC concentrations reported by Offenberg
365 et al. (2007). In this study, we only measured five out of nine monoterpene SOA tracers in Offenberg et al. (2007). Similar to
366 Ding et al. (2014), to lower the uncertainty induced from the mismatch of SOA tracer compositions, we derived a $f_{\text{SOC}_{\text{mono}}}$
367 value of 0.047 based on Offenberg et al.'s experimental data (2007) and applied it to estimate SOC_{Mono} . Many research groups
368 have adopted this tracer-based method to assess SOC productions from the five studied VOCs at various locations in the world,
369 and reasonable results have been obtained (Ding et al., 2012; Fu et al., 2014; Hu et al., 2008; Hu and Yu, 2013; Kleindienst et
370 al., 2012, 2007; Lewandowski et al., 2008).

371 As shown in Table 2, SOC estimated by the tracer-based method (SOC_{TBM}) ranged from 0.11 to 1.53 $\mu\text{gC m}^{-3}$ in Hong

372 Kong, accounting for 3.8% to 22.7% of ambient OC levels. It exhibited the same trend as OC and SOC_{PMF} , i.e., with higher
373 concentrations on regional days ($0.81 \pm 0.35 \mu\text{gC m}^{-3}$) than on LRT ($0.50 \pm 0.29 \mu\text{gC m}^{-3}$) and local days ($0.28 \pm 0.13 \mu\text{gC m}^{-3}$).
374 Similar to our previous study, monoterpenes were found to be the most significant SOC contributor in the region, with
375 SOC_{Mono} ranging from 0.05 to $0.69 \mu\text{gC m}^{-3}$ and having an average concentration of $0.23 \pm 0.17 \mu\text{gC m}^{-3}$. SOC_{Iso} and SOC_{Cary} ,
376 on the other hand, were about three times smaller than SOC_{Mono} and were $0.08 \pm 0.09 \mu\text{gC m}^{-3}$ and $0.07 \pm 0.05 \mu\text{gC m}^{-3}$,
377 respectively. Smog chamber experiments have been carried out to study the SOA yields from $\cdot\text{OH}$ oxidation, ozonolysis, and
378 nitrate radical (NO_3) oxidation of monoterpenes and isoprene, and monoterpenes were found to be more effective in SOA
379 production than isoprene (Lee et al., 2006a, 2006b). Highly oxygenated organic molecules with low and extremely low
380 volatility were formed from the oxidation of monoterpenes and observed in both laboratory experiments and field
381 measurements (Ehn et al., 2014; Jokinen et al., 2015; Zhang et al., 2018). Moreover, a synergistic $\text{O}_3 + \text{OH}$ oxidation pathway
382 of monoterpenes was recently proposed, which leads to the formation of extremely low-volatility oligomers and may result in
383 even larger monoterpene SOA yields in the real atmosphere than what observed in the smog chamber experiments (Kenseth et
384 al., 2018). Tsui et al. (2009) reported a total BVOC emission of $8.6 \times 10^9 \text{ gC yr}^{-1}$ in Hong Kong, with 40% from monoterpenes
385 and 30% from isoprene. The remaining 30% could be sesquiterpenes (e.g., β -caryophyllene) or other BVOCs. Therefore, the
386 predominance of monoterpenes SOA in BVOCs-derived SOC is likely due to the combined effects of their high SOA yields
387 and large emissions in the region. Like the SOA tracers, SOC from the four precursors all showed the highest level on regional
388 days than those on LRT and local days (Table 2). On regional days, large amounts of VOC precursors and gaseous oxidants
389 could be brought into Hong Kong through the regional transport of air masses from northern PRD and oxidized along the way.
390 Conversely, on local days, the ocean breeze brings clean air masses from the South China Sea into Hong Kong, leading to a
391 dilution effect of local air pollution. These results highlight that air mass origins play an important role in the SOC formation
392 from both biogenic and anthropogenic VOCs. Given that SOC_{TBM} is calculated based on the concentration levels of individual
393 SOA tracers measured in the ambient aerosols, it is reasonable that SOC attributed to each VOC precursor showed the same
394 meteorological variations as their SOA tracers.

395 We observed similar temporal trends between SOC_{PMF} and SOC_{TBM} ($R^2=0.71$). However, SOC_{TBM} only accounted for
396 26.5% of SOC_{PMF} , suggesting SOC must have been underestimated by the tracer-based method. A reasonable explanation is
397 that secondary formation from nighttime reactions, multi-phase reactions, and other SOA precursors are not considered in the
398 SOA tracer-based method. Parameters used in the tracer-based method were derived from pure gas-phase photo-oxidation of
399 VOC precursors in smog chambers (Kleindienst et al., 2007, 2009). Therefore, it is better to be used as a complementary
400 method with PMF in the source apportionment study of ambient OC, especially SOC.

401 3.4 Effects of anthropogenic influences on secondary aerosol formation

402 Increasing evidence from laboratory studies and ambient observations has shown that anthropogenic emissions can
403 significantly affect SOA formation from terpenoids through multiple chemical processes in both daytime and nighttime (Xu et
404 al., 2013; Zhang et al., 2018). We conducted the Pearson's R correlation analysis of all SOC terms (i.e., SOC_Iso, SOC_Mono,
405 SOC_Cary, SOC_Nap, SOC_{TBM}, SOC_{PMF}, SOC_{BB}, SOC_{SOA}, and SOC_{SS}) with O₃, NO₂, SO₂, O_X, NO₃, sulfate, particle acidity (H_p⁺),
406 and particle liquid water content (LWC_p) (Table 3). Details on the calculation of H_p⁺ and LWC_p were presented in Appendix
407 B. Since NO₃ was not directly monitored at HKEPD stations, its mixing ratio was estimated using the following equation:

$$408 \quad [NO_3] = \frac{k_1[O_3][NO_2]}{\sum k_i[VOC_i]} \quad (2)$$

409 The numerator is the production of NO₃ (p[NO₃]) from O₃ and NO₂, and the denominator is the reactivity of NO₃ for NO₃-
410 VOCs reactions. From the IUPAC database, we obtained the temperature-dependent expression of *k_l* (cm³ molecules⁻¹ s⁻¹, the
411 production rate constant of NO₃) as 1.4×10⁻¹³ exp(-2470/T), where T is the ambient temperature in Kelvin. Therefore, using *k_l*
412 and the measured concentration levels of [O₃] and [NO₂], we calculated p[NO₃] (Table 2). Brown et al. (2016) reported a NO₃-
413 VOCs reactivity of 6.5±6.8×10⁻³ s⁻¹ in Hong Kong with a corresponding NO₃ lifetime of 2.5 min. NO₃ was then calculated as
414 the ratio of p[NO₃] to this NO₃ reactivity value, and an annual mean level of 70±47 ppt was estimated.

415 As we mentioned earlier, O_X is an indicator of atmospheric oxidation capacity. Five SOC terms, i.e., SOC_Mono, SOC_Nap,
416 SOC_{TBM}, SOC_{SOA}, and SOC_{PMF}, showed significant positive correlations with O_X, especially SOC_{SOA} and SOC_{PMF} (R>0.7,
417 P<0.01). However, only SOC_{SOA} and SOC_{SS} were found to be significantly correlated with O₃ (R>0.50, P<0.01). As for NO₂,
418 another critical component of O_X, it exhibited statistically significant positive correlations with not only SOC_{SOA} and SOC_{PMF},
419 but also several TBM estimated SOCs, including SOC_{TBM}, SOC_Mono, SOC_Nap, and SOC_Cary. This may be because SOA tracers
420 used in TBM were produced from the photo-oxidation of these VOC precursors in the presence of NO_X (Kleindienst et al.,
421 2007). The significant positive correlations between NO₂ and SOC_{SOA} and SOC_{PMF} also suggest that the daytime oxidation
422 processes involving NO_X are critical SOA formation pathways in the region. Significant correlations with R>0.5 between NO₃
423 and SOC_Mono, SOC_{SOA}, SOC_{PMF}, and SOC_{SS} were also observed. BVOCs were found to account for >80% of the NO₃ reactivity
424 in Hong Kong (Brown et al., 2016), with monoterpenes as the leading contributor. Both Zhang et al. (2018) and Xu et al. (2013)
425 have reported an enhancement of nighttime monoterpenes SOA in the southeastern U.S. by NO₃-monoterpenes reactions.
426 Therefore, our findings indicate that SOA formation through nighttime NO₃ oxidation of biogenic VOCs, especially
427 monoterpenes, may have made a considerable contribution to the SOA loading in Hong Kong. However, more field
428 measurement data, e.g., quantification of the particle-phase organic nitrates using real-time online mass spectrometry
429 techniques, are needed to examine the impact of NO_X processing on SOA formation in the region.

430 Since NO₃ is a key precursor of nighttime production of HNO₃, and nitrate is a significant component of secondary inorganic
431 aerosols, it rationalized the correlations between NO₃ and SOC_{SS}. Six SOC terms, i.e., SOC_Mono, SOC_Nap, SOC_{TBM}, SOC_{SOA},
432 SOC_{SS}, and SOC_{PMF}, showed significant positive correlations with sulfate, especially SOC_{SS} and SOC_{PMF} (R≥0.8, P<0.01).

433 Given that sulfate is the key component of secondary inorganic aerosol, such a strong correlation between SOC_{SS} and sulfate
434 is expected. Moreover, several studies have suggested that sulfate also plays a dominant role in the production of aerosol-phase
435 organosulfates through both nucleophilic addition reactions and the salting-in effect (Lin et al., 2012; Riva et al., 2015; Xu et
436 al., 2015).

437 We then performed multivariate linear regression (MLR) analysis to obtain a quantitative and comprehensive understanding
438 of the impacts of gaseous oxidants and aerosol characteristics on SOC_{TBM}, SOC_{PMF}, and the individual PMF resolved SOCs
439 (i.e., SOC_{SS}, SOC_{SOA}, and SOC_{BB}). Six parameters, namely O₃, NO₂, NO₃, sulfate, H_p⁺, and LWC_p, were included in the
440 preliminary runs. However, the MLR results showed that O₃ was an insignificant factor for all SOC terms, even with negative
441 regression coefficients. Pearson's R analysis also showed that SOC was more NO₂ dependent than O₃. Therefore, it was
442 excluded from the final MLR analysis, and the results were shown in Table 4.

443 We found that two parameters, i.e., sulfate and NO₃, have statistically significant positive linear relationships ($P \leq 0.001$)
444 with SOC_{SS}, and the regression coefficients were 0.913 and 0.234, respectively. The result is reasonable and consistent with
445 what was observed from Pearson's R analysis, given that sulfate is the critical component in the PMF resolved SS factor, and
446 NO₃ is the precursor of nitrate through HNO₃ formation at nighttime. As for SOC_{BB}, three parameters, i.e., NO₂, NO₃, and
447 H_p⁺, showed significant linear relationships with it ($P < 0.01$), with a regression coefficient of 0.639, -0.509, and 0.503,
448 respectively. This indicates that a 1 mol L⁻¹ increase in particle acidity was associated with a 0.503 μgC m⁻³ increase in SOC
449 from BB aging. Phenols, which are produced from the combustion of lignin, are a typical class of gaseous compounds emitted
450 in large amounts from BB (Bruns et al., 2016; Schauer et al., 2001). Recent laboratory studies indicate that phenols can undergo
451 multi-phase photochemical reactions in the atmosphere with the formation of nitrophenols and nitrocatechols (Finewax et al.,
452 2018; Yu et al., 2014). Vione et al. (2001) observed the aqueous phase photonitration of phenols, which was pH-dependent
453 with more nitro-compounds generated at lower pH. Given the strong particle acidity (pH annual mean: -0.28) observed in the
454 Hong Kong atmosphere, the formation of the 4-nitrocatechol and its analogs may be favored in the BB plume, which enhances
455 SOC_{BB} formation.

456 Both sulfate and NO₂ were found as the statistically significant factors that positively correlated with SOC_{PMF}, with
457 regression coefficients of 0.530 and 0.373, respectively ($P < 0.001$, Table 4). This suggests reducing the sulfate level by 1 μg
458 m⁻³ and NO₂ level by 1 ppb could lower the total PMF-apportioned SOC by 0.530 and 0.373 μgC m⁻³, respectively. NO₂ was
459 also the most significant factor influencing SOC_{TBM}, with a regression coefficient of 0.383 ($P < 0.001$), indicating that a decrease
460 of NO₂ by 1 ppb can reduce SOC_{TBM} by 0.383 μgC m⁻³. As for SOC_{SOA}, we found NO₃ as the most significant parameter
461 ($P < 0.01$), and a decrease of 1 ppb NO₃ can lead to a reduction of SOC_{SOA} by 0.384 μgC m⁻³ when holding other covariates
462 unchanged. These results are consistent with what was observed from Pearson's R analysis, indicating the importance of NO_x
463 processing on both daytime and nighttime SOA production in the region.

464 4 Conclusions

465 In this study, we identified and quantitatively assessed the contributions of six primary and secondary sources to ambient
466 OC in Hong Kong, and secondary formation was found to be the leading contributor. Anthropogenic emissions, including NO₂,
467 O_x, NO₃, and sulfate, significantly influenced SOA formation in the region. In particular, NO_x processing in both daytime and
468 nighttime has played a critical role. Although the ambient NO₂ level has dropped by 33.3% from 1999 to 2019 (the government
469 of HKSAR, <https://www.info.gov.hk/gia/general/202001/20/P2020012000874.htm>) and sulfate level in PM_{2.5} was also
470 lowered by about 30% from 2000 to 2016 (HKEPD, 2017), the roadside NO₂ level was still high. According to the 20-year air
471 pollutants monitoring data released by HKSAR, the annual average concentration of roadside NO₂ was much higher than the
472 other gaseous pollutants, and it peaked during 2011-2013, which were 122 and 118 μg m⁻³ in 2011 and 2012, respectively.
473 Although the annual ambient level of roadside NO₂ decreased to 80 μg m⁻³ in 2019, it is still two times higher than the annual
474 objective level set by the HKSAR government, indicating a continuous significant impact of NO_x on SOA formation in Hong
475 Kong, especially in areas with heavy traffic load. Given that 90% of the roadside NO₂ was from commercial vehicles, such as
476 buses, trucks, minibuses, and so on, our results suggest that more stringent control of NO_x emission from commercial vehicles
477 is needed. This will benefit the community by reducing not only the background NO_x levels but also the SOA pollution in
478 Hong Kong.

479 Appendices

480 Appendix A: Kinetic model of loss of isoprene intermediates

481 In this study, we use Kintecus (Ianni, 2015), a kinetics simulation software, to investigate the degradation pathways of two
482 isoprene SOA intermediates, i.e., IEPOX and MAE, in the atmosphere. Simulation time was set to be 100 h to ensure the
483 completion of reactions. As described by Eddingsass et al. (2010) and Worton et al. (2013), IEPOX and MAE are removed
484 from the atmosphere mainly through three pathways, namely the gas-phase photo-oxidation, dry deposition, and aerosol phase
485 acid-catalyzed ring-opening reaction. Reaction constants that are involved in these three degradation processes were listed
486 below.

IEPOX:

$$k_{\text{OX}} = 5.78 \times 10^{-11} \cdot e^{-400/T} \cdot [\text{OH}] \text{ s}^{-1}$$

$$k_{\text{dd}} = dv/blh \text{ s}^{-1}$$

$$k_{\text{H}^+} = 5 \times 10^{-2} \cdot [\text{H}_p^+] \text{ s}^{-1}$$

$$k_{\text{H}}^{\text{CP}} = 1.3 \times 10^8 \text{ M atm}^{-1}$$

MAE:

$$k'_{\text{OX}} = 1.0 \times 10^{-12} \cdot [\text{OH}] \text{ s}^{-1}$$

$$k'_{\text{dd}} = dv/blh \text{ s}^{-1}$$

$$k'_{\text{H}^+} = 5.91 \times 10^{-5} \cdot [\text{H}_p^+] \text{ s}^{-1}$$

$$k'_{\text{H}}^{\text{CP}} = 7.5 \times 10^6 \text{ M atm}^{-1}$$

487 The eight terms, i.e., k_{OX} and k'_{OX} , k_{dd} and k'_{dd} , k_{H^+} and k'_{H^+} , and k_{H}^{CP} and $k'_{\text{H}}^{\text{CP}}$, are the gas-phase oxidation rate
488 constants, dry deposition rate constants, acid-catalyzed ring-opening rate constants, and Henry's law constants of IEPOX and

489 MAE, respectively. Given the annual average OH radical level in the PRD region was 5×10^6 molecules cm^{-3} (Hofzumahaus et
 490 al., 2009), k_{OX} and k'_{OX} were calculated to be $7.55 \times 10^{-5} \text{ s}^{-1}$ and $5.12 \times 10^{-6} \text{ s}^{-1}$ at 298 K. k_{dd} is estimated by the deposition
 491 velocity (dv) and the boundary layer height (blh). Like Eddingsaas et al. (2010) and Worton et al. (2013), we assumed the same
 492 deposition velocities for IEPOX and MAE as that for hydrogen peroxide ($1\text{-}5 \text{ cm s}^{-1}$). With the predicted boundary height in
 493 Hong Kong of 1100 m (Xie et al., 2012), k_{dd} and k'_{dd} were calculated to be $5.05 \times 10^{-5} \text{ s}^{-1}$. Given the high volatility of MAE
 494 vapor pressure ($9.2 \times 10^{-5} \text{ atm}$) (Worton et al., 2013), it has a low tendency to partition onto the particle phase, and its uptake
 495 onto aqueous particles is mainly governed by Henry's law constant (k_{H}^{CP}). Worton et al. (2013) estimated the k_{H}^{CP} value of
 496 MAE to be $7.5 \times 10^6 \text{ M atm}^{-1}$, which is 20 times lower than that of IEPOX ($1.3 \times 10^8 \text{ M atm}^{-1}$, Minerath et al., 2008). Moreover,
 497 Riedel et al. (2015) suggested that the heterogeneous reactive uptake coefficient of MAE ($\gamma = 4.9 \times 10^{-4}$) through the ring-
 498 opening reaction was a factor of 30 lower than that of IEPOX. The ring-opening rate constant (k_{H^+}) for IEPOX and MAE were
 499 estimated by Eddingsaas et al. (2010) and Birdsall et al. (2014), which are $5 \times 10^{-2} \text{ M}^{-1} \text{ s}^{-1}$ and $5.91 \times 10^{-5} \text{ M}^{-1} \text{ s}^{-1}$, respectively.
 500 We then inputted all these parameters into the Kintecus model and estimated the fractions of IEPOX and MAE degraded
 501 through the above-mentioned three pathways.

502 **Appendix B: Calculation of particle acidity and total liquid water content**

503 A thermodynamic *model (E-AIM model II)* was applied to estimate the hydrogen ion concentration in air (H^+_{air}) and liquid
 504 water content associated with inorganic species ($\text{LWC}_{\text{inorg}}$). The liquid water content associated with organic species (LWC_{org})
 505 was calculated using the following equation

$$506 \quad \text{LWC}_{\text{org}} = \frac{m_{\text{org}} \rho_w}{\rho_{\text{org}}} \frac{k_{\text{org}}}{(1/\text{RH} - 1)}$$

507 where k_{org} is an organic hygroscopicity parameter and has a value of 0.1, m_{org} is organic mass concentration, and a factor
 508 of 2.1 was applied to convert OC to OM at the urban location. ρ_w is the water density, and a typical value of 1.4 g cm^{-1} was
 509 applied for organic aerosols (ρ_{org}). Since LWC is associated with both inorganic and organic species, the total particle water
 510 (LWC_p) was calculated as the sum of $\text{LWC}_{\text{inorg}}$ and LWC_{org} based on the assumption that particles were internally well mixed.

511 Particle acidity was calculated using the following equation:

$$512 \quad \text{H}^+_p = \frac{1000 \text{H}^+_{\text{air}}}{\text{LWC}_{\text{org}} + \text{LWC}_{\text{inorg}}}$$

513 where H^+_p (mol L^{-1}) is the concentration of hydrogen ion in aerosol water, interpreted as particle acidity. H^+_{air} and $\text{LWC}_{\text{inorg}}$
 514 were calculated by E-AIM model II using input values of inorganic ions, RH, and temperature.

515 **Data availability.** Raw data used in this study are archived at Hong Kong Baptist University, and are available upon request
 516 by contacting the corresponding author.

517 **Author contributions.** YBC and DH designed the study. YBC did all the experiments and most of the data analysis. YQM
 518 helped with regression analysis and data interpretation. YBC drafted the manuscript. DH helped with data analysis and

519 interpretation and revised the manuscript.

520 **Competing interest.** The authors declare that they have no conflict of interest.

521

522 **Acknowledgment**

523 This work was supported by the National Natural Science Foundation of China (21976151 and 21477102) and the General
524 Research Fund of Hong Kong Research Grant Council (12328216, 12304215, 12300914). The authors thank the
525 Environmental Central Facility (ENVF) in Hong Kong University of Science and Technology (HKUST) for real-time
526 environmental and air quality data (<http://envf.ust.hk/dataview/gts/current/>).

527 **References**

- 528 An, Z., Huang, R.J., Zhang, R., Tie, X., Li, G., Cao, J., Zhou, W., Shi, Z., Han, Y., Gu, Z., Ji, Y.: Severe haze in northern China:
529 A synergy of anthropogenic emissions and atmospheric processes, *Proc. Natl. Acad. Sci. U. S. A.*, 116, 8657–8666,
530 <https://doi.org/10.1073/pnas.1900125116>, 2019.
- 531 Barbara J. Finlayson-Pitts, James N. Pitts, J.: Chemistry of the upper and lower atmosphere, Academic Press,
532 <https://doi.org/https://doi.org/10.1016/B978-0-12-257060-5.X5000-X>, 2000.
- 533 Birdsall, A.W., Miner, C.R., Mael, L.E., Elrod, M.J.: Mechanistic study of secondary organic aerosol components formed from
534 nucleophilic addition reactions of methacrylic acid epoxide, *Atmos. Chem. Phys.*, 14, 12951–12964,
535 <https://doi.org/10.5194/acp-14-12951-2014>, 2014.
- 536 Brown, S.S., Dubé, W.P., Bahreini, R., Middlebrook, A.M., Brock, C.A., Warneke, C., De Gouw, J.A., Washenfelder, R.A.,
537 Atlas, E., Peischl, J., Ryerson, T.B., Holloway, J.S., Schwarz, J.P., Spackman, R., Trainer, M., Parrish, D.D., Fehsenfeld,
538 F.C., Ravishankara, A.R.: Biogenic VOC oxidation and organic aerosol formation in an urban nocturnal boundary layer:
539 Aircraft vertical profiles in Houston, TX, *Atmos. Chem. Phys.*, 13, 11317–11337. [https://doi.org/10.5194/acp-13-11317-](https://doi.org/10.5194/acp-13-11317-2013)
540 2013, 2013.
- 541 Brown, S.S., Dubé, W.P., Tham, Y.J., Zha, Q.Z., Xue, L.K., Poon, S., Wang, Z., Blake, D.R., Tsui, W., Parrish, D.D., Wang, T.:
542 Nighttime chemistry at a high altitude site above Hong Kong, *J. Geophys. Res. Atmos.*, 121, 2457–2475, doi:10.1002/
543 2015JD024566, 2016.
- 544 Bruns, E.A., El Haddad, I., Slowik, J.G., Kilic, D., Klein, F., Baltensperger, U., Prévôt, A.S.H.: Identification of significant
545 precursor gases of secondary organic aerosols from residential wood combustion, *Sci. Rep.*, 6, 27881.
546 <https://doi.org/10.1038/srep27881>, 2016.
- 547 Chan, M.N., Surratt, J.D., Claeys, M., Edgerton, E.S., Tanner, R.L., Shaw, S.L., Zheng, M., Knipping, E.M., Eddingsaas, N.C.,
548 Wennberg, P.O., Seinfeld, J.H.: Characterization and quantification of isoprene-derived epoxydiols in ambient aerosol
549 in the southeastern united states, *Environ. Sci. Technol.*, 44, 4590–4599, <https://doi.org/10.1021/es100596b>, 2010.
- 550 Cheng, Y., Ma, Y., Dong, B., Qiu, X., Hu, D.: Pollutants from primary sources dominate the oxidative potential of water-
551 soluble PM_{2.5} in Hong Kong in terms of dithiothreitol (DTT) consumption and hydroxyl radical production, *J. Hazard.*
552 *Mater.*, 405, 124218, doi:10.1016/j.jhazmat.2020.124218, 2021.
- 553 Ding, X., Wang, X.M., Gao, B., Fu, X.X., He, Q.F., Zhao, X.Y., Yu, J.Z., Zheng, M.: Tracer-based estimation of secondary
554 organic carbon in the Pearl River Delta, South China, *J. Geophys. Res. Atmos.*, 117, D05313,
555 <https://doi.org/10.1029/2011JD016596>, 2012.
- 556 Ding, X., He, Q., Shen, R., Yu, Q., Wang, X., Guenther, D., Dlugokencky, E., Lang, P., Newberger, T., Wolter, S., White, A.,
557 Noone, D., Wolfe, D., Schnell, R., Ding, X., He, Q., Shen, R., Yu, Q., Wang, X.: Spatial distributions of secondary
558 organic aerosols from isoprene, monoterpenes, β -caryophyllene, and aromatics over China during summer, *J. Geophys.*
559 *Res. Atmos.*, 119, 11877–11891, <https://doi.org/10.1002/2014JD02174>, 2014.
- 560 Eddingsaas, N.C., Vandernelde, D.G., Wennberg, P.O.: Kinetics and products of the acid-catalyzed ring-opening of
561 atmospherically relevant butyl epoxy alcohols, *J. Phys. Chem. A*, 114, 8106–8113, <https://doi.org/10.1021/jp103907c>,
562 2010.
- 563 Ehn, M., Thornton, J.A., Kleist, E., Sipilä, M., Junninen, H., Pullinen, I., Springer, M., Rubach, F., Tillmann, R., Lee, B.,
564 Lopez-Hilfiker, F., Andres, S., Acir, I.H., Rissanen, M., Jokinen, T., Schobesberger, S., Kangasluoma, J., Kontkanen, J.,
565 Nieminen, T., Kurtén, T., Nielsen, L.B., Jørgensen, S., Kjaergaard, H.G., Canagaratna, M., Maso, M.D., Berndt, T., Petäjä,
566 T., Wahner, A., Kerminen, V.M., Kulmala, M., Worsnop, D.R., Wildt, J., Mentel, T.F.: A large source of low-volatility
567 secondary organic aerosol, *Nature*, 506, 476–479, <https://doi.org/10.1038/nature13032>, 2014.
- 568 Environmental Protection Department of Hong Kong, Hong Kong emission inventory report.
569 https://www.epd.gov.hk/epd/sc_chi/environmentinhk/air/data/emission_inve.html, 2017.

570 Finewax, Z., De Gouw, J.A., Ziemann, P.J.: Identification and quantification of 4-nitrocatechol formed from OH and NO₃
571 radical-initiated reactions of catechol in air in the presence of NO_x: Implications for secondary organic aerosol formation
572 from biomass burning, *Environ. Sci. Technol.*, 52, 1981–1989, <https://doi.org/10.1021/acs.est.7b05864>, 2018.

573 Fry, J.L., Rollins, a W., Wooldridge, P.J., Brown, S.S., Fuchs, H., Dub, W.: Organic nitrate and secondary organic aerosol
574 yield from NO₃ oxidation of β-pinene evaluated using a gas-phase kinetics/aerosol partitioning model, *Atmos. Chem.
575 Phys.*, 9, 1431–1449, <https://doi.org/10.5194/acp-9-1431-2009>, 2009.

576 Fu, P., Kawamura, K., Chen, J., Miyazaki, Y.: Secondary production of organic aerosols from biogenic VOCs over Mt. Fuji,
577 Japan, *Environ. Sci. Technol.*, 48, 8491–8497, <https://doi.org/10.1021/es500794d>, 2014.

578 Gelencsér, A., May, B., Simpson, D., Sánchez-Ochoa, A., Kasper-Giebl, A., Puxbaum, H., Caseiro, A., Pio, C.A., Legrand, M.:
579 Source apportionment of PM_{2.5} organic aerosol over Europe: Primary/secondary, natural/anthropogenic, and
580 fossil/biogenic origin, *J. Geophys. Res. Atmos.* 112, 1–12, <https://doi.org/10.1029/2006JD008094>, 2007.

581 He, Q.F., Ding, X., Fu, X.X., Zhang, Y.Q., Wang, J.Q., Liu, Y.X., Tang, M.J., Wang, X.M., Rudich, Y., Secondary organic
582 aerosol formation from isoprene epoxides in the Pearl River Delta, South China: IEPOX- and HMML-derived tracers,
583 *J. Geophys. Res. Atmos.*, 123, 6999–7012, <https://doi.org/10.1029/2017JD028242>, 2018.

584 He, X., Huang, X.H.H., Chow, K.S., Wang, Q., Zhang, T., Wu, D., Yu, J.Z.: Abundance and sources of phthalic acids, benzene-
585 tricarboxylic acids, and phenolic acids in PM_{2.5} at urban and suburban sites in Southern China, *ACS Earth Sp. Chem.*, 2,
586 147–158, <https://doi.org/10.1021/acsearthspacechem.7b00131>, 2018.

587 Hildemann, L.M., Rogge, W.F., Cass, G.R., Mazurek, M.A., Simoneit, B.R.T.: Contribution of primary aerosol emissions from
588 vegetation-derived sources to fine particle concentrations in Los Angeles, *J. Geophys. Res.*, 101, 19541,
589 <https://doi.org/10.1029/95JD02136>, 1996.

590 Hofzumahaus, A., Rohrer, F., Lu, K., Bohn, B., Brauers, T., Chang, C.-C., Fuchs, H., Holland, F., Kita, K., Kondo, Y., Li, X.,
591 Lou, S., Shao, M., Zeng, L., Wahner, A., Zhang, Y.: Amplified trace gas removal in the troposphere, *Science*, 324, 1702–
592 1704, <https://doi.org/10.1126/science.1164566>, 2009.

593 Hu, D., Yu, J. Z.: Secondary organic aerosol tracers and malic acid in Hong Kong: Seasonal trends and origins, *Environ. Chem.*,
594 10, 381–394, <https://doi.org/10.1071/EN13104>, 2013.

595 Hu, D., Bian, Q., Li, T.W.Y., Lau, A.K.H., Yu, J.Z.: Contributions of isoprene, monoterpenes, β-caryophyllene, and toluene to
596 secondary organic aerosols in Hong Kong during the summer of 2006, *J. Geophys. Res. Atmos.*, 113,
597 <https://doi.org/10.1029/2008JD010437>, 2008.

598 Hu, D., Bian, Q., Lau, A.K.H., Yu, J.Z.: Source apportioning of primary and secondary organic carbon in summer PM_{2.5} in
599 Hong Kong using positive matrix factorization of secondary and primary organic tracer data, *J. Geophys. Res. Atmos.*,
600 115, 1–14, <https://doi.org/10.1029/2009JD012498>, 2010.

601 Huang, R.J., Zhang, Y., Bozzetti, C., Ho, K.F., Cao, J.J., Han, Y., Daellenbach, K.R., Slowik, J.G., Platt, S.M., Canonaco, F.,
602 Zotter, P., Wolf, R., Pieber, S.M., Bruns, E.A., Crippa, M., Ciarelli, G., Piazzalunga, A., Schwikowski, M., Abbaszade,
603 G., Schnelle-Kreis, J., Zimmermann, R., An, Z., Szidat, S., Baltensperger, U., El Haddad, I., Prevot, A.S.: High secondary
604 aerosol contribution to particulate pollution during haze events in China, *Nature*, 514, 218–222,
605 <https://doi.org/10.1038/nature13774>, 2014.

606 Ianni, J.C.: KINTECUS, Windows version 5.50, 2015.

607 Jang, M., Czoschke, N.M., Lee, S., Kamens, R.M.: Heterogeneous atmospheric aerosol production by acid-catalyzed particle-
608 phase reactions, *Science*, 298, 814–817, <https://doi.org/10.1126/science.1075798>, 2002.

609 Jaoui, M., Kleindienst, T.E., Lewandowski, M., Offenberg, J.H., Edney, E.O.: Identification and quantification of aerosol polar
610 oxygenated compounds bearing carboxylic or hydroxyl groups. 2. Organic tracer compounds from monoterpenes,
611 *Environ. Sci. Technol.*, 39, 5661–5673, <https://doi.org/10.1021/es048111b>, 2005.

612 Jokinen, T., Berndt, T., Makkonen, R., Kerminen, V.M., Junninen, H., Paasonen, P., Stratmann, F., Herrmann, H., Guenther,

613 A.B., Worsnop, D.R., Kulmala, M., Ehn, M., Sipilä, M.: Production of extremely low volatile organic compounds from
614 biogenic emissions: Measured yields and atmospheric implications, *Proc. Natl. Acad. Sci. U. S. A.*, 112, 7123–7128,
615 <https://doi.org/10.1073/pnas.1423977112>, 2015.

616 Kanakidou, M., Seinfeld, J.H., Pandis, S.N., Barnes, I., Dentener, F.J., Facchini, M.C., Van Dingenen, R., Ervens, B., Nenes,
617 A., Nielsen, C.J., Swietlicki, E., Putaud, J.P., Balkanski, Y., Fuzzi, S., Horth, J., Moortgat, G.K., Winterhalter, R., Myhre,
618 C.E.L., Tsigaridis, K., Vignati, E., Stephanou, E.G., Wilson, J.: Organic aerosol and global climate modelling: a review,
619 *Atmos. Chem. Phys.*, 5, 1053–1123, <https://doi.org/10.5194/acp-5-1053-2005>, 2005.

620 Kautzman, K.E., Surratt, J.D., Chan, M.N., Chan, A.W.H., Hersey, S.P., Chhabra, P.S., Dalleska, N.F., Wennberg, P.O., Flagan,
621 R.C., Seinfeld, J.H.: Chemical composition of gas- and aerosol-phase products from the photooxidation of naphthalene,
622 *J. Phys. Chem. A*, 114, 913–934, <https://doi.org/10.1021/jp908530s>, 2010.

623 Kenseth, C.M., Huang, Y., Zhao, R., Dalleska, N.F., Caleb Hethcox, J., Stoltz, B.M., Seinfeld, J.H.: Synergistic O₃+OH
624 oxidation pathway to extremely low-volatility dimers revealed in β-pinene secondary organic aerosol, *Proc. Natl. Acad.*
625 *Sci. U. S. A.*, 115, 8301–8306, <https://doi.org/10.1073/pnas.1804671115>, 2018.

626 Kitanovski, Z., Grgić, I., Vermeylen, R., Claeys, M., Maenhaut, W.: Liquid chromatography tandem mass spectrometry method
627 for characterization of monoaromatic nitro-compounds in atmospheric particulate matter, *J. Chromatogr. A*, 1268, 35–
628 43, <https://doi.org/10.1016/j.chroma.2012.10.021>, 2012.

629 Kleindienst, T.E., Jaoui, M., Lewandowski, M., Offenberg, J.H., Lewis, C.W., Bhave, P. V., Edney, E.O.: Estimates of the
630 contributions of biogenic and anthropogenic hydrocarbons to secondary organic aerosol at a southeastern US location,
631 *Atmos. Environ.*, 41, 8288–8300, <https://doi.org/10.1016/j.atmosenv.2007.06.045>, 2007.

632 Kleindienst, T.E., Lewandowski, M., Offenberg, J.H., Jaoui, M., Edney, E.O.: The formation of secondary organic aerosol
633 from the isoprene + OH reaction in the absence of NO_x, *Atmos. Chem. Phys.*, 9, 6541–6558, [https://doi.org/10.5194/acp-](https://doi.org/10.5194/acp-9-6541-2009)
634 [9-6541-2009](https://doi.org/10.5194/acp-9-6541-2009), 2009.

635 Kleindienst, T.E., Jaoui, M., Lewandowski, M., Offenberg, J.H., Docherty, K.S.: The formation of SOA and chemical tracer
636 compounds from the photo-oxidation of naphthalene and its methyl analogs in the presence and absence of nitrogen
637 oxides, *Atmos. Chem. Phys.*, 12, 8711–8726, <https://doi.org/10.5194/acp-12-8711-2012>, 2012.

638 Lee, A., Goldstein, A.H., Keywood, M.D., Gao, S., Varutbangkul, V., Bahreini, R., Ng, N.L., Flagan, R.C., Seinfeld, J.H.: Gas-
639 phase products and secondary aerosol yields from the ozonolysis of ten different terpenes, *J. Geophys. Res. Atmos.*, 111,
640 1–18, <https://doi.org/10.1029/2005JD006437>, 2006a.

641 Lee, A., Goldstein, A.H., Kroll, J.H., Ng, N.L., Varutbangkul, V., Flagan, R.C., Seinfeld, J.H.: Gas-phase products and
642 secondary aerosol yields from the photo-oxidation of 16 different terpenes, *J. Geophys. Res. Atmos.*, 111, D17305,
643 <https://doi.org/10.1029/2006JD007050>, 2006b.

644 Lewandowski, M., Jaoui, M., Offenberg, J.H., Kleindienst, T.E., Edney, E.O., Sheesley, R. J., Schauer, J.J.: Primary and
645 secondary contributions to ambient PM in the midwestern united states, *Environ. Sci. Technol.*, 42, 3303–3309,
646 <https://doi.org/10.1021/es0720412>, 2008.

647 Lin, Y.-H., Zhang, Z., Docherty, K.S., Zhang, H., Budisulistiorini, S.H., Rubitschun, C.L., Shaw, S.L., Knipping, E.M.,
648 Edgerton, E.S., Kleindienst, T.E., Gold, A., Surratt, J.D.: Isoprene epoxydiols as precursors to secondary organic aerosol
649 formation: Acid-catalyzed reactive uptake studies with authentic compounds, *Environ. Sci. Technol.*, 46, 250–258,
650 <https://doi.org/10.1021/es202554c>, 2012.

651 Lin, Y.-H., Zhang, H., Pye, H.O.T., Zhang, Z., Marth, W.J., Park, S., Arashiro, M., Cui, T., Budisulistiorini, S.H., Sexton, K.G.,
652 Vizueté, W., Xie, Y., Luecken, D.J., Piletic, I.R., Edney, E.O., Bartolotti, L.J., Gold, A., Surratt, J.D.: Epoxide as a
653 precursor to secondary organic aerosol formation from isoprene photo-oxidation in the presence of nitrogen oxides, *Proc.*
654 *Natl. Acad. Sci. U. S. A.*, 110, 6718–6723, <https://doi.org/10.1073/pnas.1221150110>, 2013.

655 Lu, X., Fung, J.: Source apportionment of sulfate and nitrate over the Pearl River Delta Region in China, *Atmosphere*, 7, 98,

656 <https://doi.org/10.3390/atmos7080098>, 2016.

657 Ma, Y., Cheng, Y., Qiu, X., Lin, Y., Cao, J., Hu, D.: A quantitative assessment of source contributions to fine particulate matter
658 (PM_{2.5})-bound polycyclic aromatic hydrocarbons (PAHs) and their nitrated and hydroxylated derivatives in Hong Kong,
659 Environ. Pollut., 219, 742-749, <https://doi.org/10.1016/j.envpol.2016.07.034>, 2016.

660 Ma, Y., Cheng, Y., Qiu, X., Cao, G., Fang, Y., Wang, J., Zhu, T., Yu, J., Hu, D.: Sources and oxidative potential of water-soluble
661 humic-like substances (HULIS_{WS}) in fine particulate matter (PM_{2.5}) in Beijing, Atmos. Chem. Phys., 18, 5607-5617,
662 <https://doi.org/10.5194/acp-18-5607-2018>, 2018.

663 Ma, Y., Cheng, Y., Qiu, X., Cao, G., Kuang, B., Yu, J.Z., Hu, D.: Optical properties, source apportionment and redox activity
664 of humic-like substances (HULIS) in airborne fine particulates in Hong Kong, Environ. Pollut., 255, 113087,
665 <https://doi.org/10.1016/j.envpol.2019.113087>, 2019.

666 Mancilla, Y., Herckes, P., Fraser, M.P., Mendoza, A.: Secondary organic aerosol contributions to PM_{2.5} in Monterrey, Mexico:
667 Temporal and seasonal variation, Atmos. Res., 153, 348–359, <https://doi.org/10.1016/j.atmosres.2014.09.009>, 2015.

668 Minerath, E. C., Casale, M. T., Elrod, M. J.: Kinetics feasibility study of alcohol sulfate esterification reactions in tropospheric
669 aerosols, Environ. Sci. Technol., 42, 4410–4415, <https://doi.org/10.1021/es8004333>, 2008.

670 Ng, N.L., Kwan, A.J., Surratt, J.D., Chan, A.W.H., Chhabra, P.S., Sorooshian, A., Pye, H.O.T., Crouse, J.D., Wennberg, P.O.,
671 Flagan, R.C., Seinfeld, J.H.: Secondary organic aerosol (SOA) formation from reaction of isoprene with nitrate radicals
672 (NO₃), Atmos. Chem. Phys., 8, 4117–4140, <https://doi.org/10.5194/acp-8-4117-2008>, 2008.

673 Nguyen, T.B., Bates, K.H., Crouse, J.D., Schwantes, R.H., Zhang, X., Kjaergaard, H.G., Surratt, J.D., Lin, P., Laskin, A.,
674 Seinfeld, J.H., Wennberg, P.O.: Mechanism of the hydroxyl radical oxidation of methacryloyl peroxyxynitrate (MPAN)
675 and its pathway toward secondary organic aerosol formation in the atmosphere, Phys. Chem. Chem. Phys., 17, 17914–
676 17926, <https://doi.org/10.1039/c5cp02001h>, 2015.

677 Offenberg, J. H., Lewis, C. W., Lewandowski, M., Jaoui, M., Kleindienst, T. E., Edney, E. O.: Contributions of toluene and α -
678 pinene to SOA formed in an irradiated toluene/ α -pinene/NO_x/air mixture: comparison of results using ¹⁴C content and
679 SOA organic tracer methods, Environ. Sci. Technol., 41, 3972-3976, <https://doi.org/10.1021/es070089>, 2007.

680 Rattanavaraha, W., Chu, K., Budisulistiorini, S.H., Riva, M., Lin, Y.H., Edgerton, E.S., Baumann, K., Shaw, S.L., Guo, H.,
681 King, L., Weber, R.J., Neff, M.E., Stone, E.A., Offenberg, J.H., Zhang, Z., Gold, A., Surratt, J.D.: Assessing the impact
682 of anthropogenic pollution on isoprene-derived secondary organic aerosol formation in PM_{2.5} collected from the
683 Birmingham, Alabama, ground site during the 2013 Southern Oxidant and Aerosol Study, Atmos. Chem. Phys., 16,
684 4897–4914, <https://doi.org/10.5194/acp-16-4897-2016>, 2016.

685 Riedel, T.P., Lin, Y.H., Budisulistiorini, S.H., Gaston, C.J., Thornton, J.A., Zhang, Z., Vizuete, W., Gold, A., Surratt, J.D.:
686 Heterogeneous reactions of isoprene-derived epoxides: Reaction probabilities and molar secondary organic aerosol yield
687 estimates, Environ. Sci. Technol. Lett., 2, 38–42, <https://doi.org/10.1021/ez500406f>, 2015.

688 Riva, M., Tomaz, S., Cui, T., Lin, Y.H., Perraudin, E., Gold, A., Stone, E.A., Villenave, E., Surratt, J.D.: Evidence for an
689 unrecognized secondary anthropogenic source of organosulfates and sulfonates: Gas-phase oxidation of polycyclic
690 aromatic hydrocarbons in the presence of sulfate aerosol, Environ. Sci. Technol., 49, 6654–6664,
691 <https://doi.org/10.1021/acs.est.5b00836>, 2015.

692 Roberts, J.M., Bertman, S.B.: The thermal decomposition of peroxyacetic nitric anhydride (PAN) and peroxyacrylic nitric
693 anhydride (MPAN), Int. J. Chem. Kinet., 24, 297–307, <https://doi.org/10.1002/kin.550240307>, 1992.

694 Rollins, A.W., Pusede, S., Wooldridge, P., Min, K.-E., Gentner, D. R., Goldstein, A.H., Liu, S., Day, D. A., Russell, L. M.,
695 Rubitschun, C. L., Surratt, J. D., Cohen, R.C.: Gas particle partitioning of total alkyl nitrates observed with TD-LIF in
696 Bakersfield, J. Geophys. Res. Atmos., 118, 6651–6662, <https://doi.org/10.1002/jgrd.50522>, 2013.

697 Sang, X.F., Chan, C.Y., Engling, G., Chan, L.Y., Wang, X.M., Zhang, Y.N., Shi, S., Zhang, Z.S., Zhang, T., Hu, M.:
698 Levoglucosan enhancement in ambient aerosol during springtime transport events of biomass burning smoke to

699 Southeast China, *Tellus B*, 63, 129–139, <https://doi.org/10.1111/j.1600-0889.2010.00515.x>, 2011.

700 Schauer, J.J., Kleeman, M.J., Cass, G.R., Simoneit, B.R.T.: Measurement of emissions from air pollution sources. 3. C₁-C₂₉
701 organic compounds from fireplace combustion of wood, *Environ. Sci. Technol.*, 35, 1716–1728,
702 <https://doi.org/10.1021/es001331e>, 2001.

703 Schauer, J.J., Rogge, W.F., Hildemann, L.M., Mazurek, M.A., Cass, G.R., Simoneit, B.R.T.: Source apportionment of airborne
704 particulate matter using organic compounds as tracers, *Atmos. Environ.*, 41, 241–259,
705 <https://doi.org/10.1016/j.atmosenv.2007.10.069>, 2007.

706 Simoneit, B.R.T.: A review of biomarker compounds as source indicators and tracers for air pollution, *Environ. Sci. Pollut.*
707 *Res.*, 6, 159–169, <https://doi.org/10.1007/BF02987621>, 1999.

708 Simoneit, B.R.T., Medeiros, P.M., Didyk, B.M.: Combustion products of plastics as indicators for refuse burning in the
709 atmosphere, *Environ. Sci. Technol.*, 39, 6961–6970, <https://doi.org/10.1021/es050767x>, 2005.

710 Surratt, J.D., Chan, A.W.H., Eddingsaas, N.C., Chan, M., Loza, C.L., Kwan, A.J., Hersey, S.P., Flagan, R.C., Wennberg, P.O.,
711 Seinfeld, J.H.: Reactive intermediates revealed in secondary organic aerosol formation from isoprene, *Proc. Natl. Acad.*
712 *Sci. U. S. A.*, 107, 6640–6645, <https://doi.org/10.1073/pnas.0911114107>, 2010.

713 Tsui, J.K.Y., Guenther, A., Yip, W.K., Chen, F.: A biogenic volatile organic compound emission inventory for Hong Kong,
714 *Atmos. Environ.*, 43, 6442–6448, <https://doi.org/10.1016/j.atmosenv.2008.01.027>, 2009.

715 Van Dingenen, R., Raes, F., Putaud, J.P., Baltensperger, U., Charron, A., Facchini, M.C., Decesari, S., Fuzzi, S., Gehrig, R.,
716 Hansson, H.C., Harrison, R.M., Hüglin, C., Jones, A.M., Laj, P., Lorbeer, G., Maenhaut, W., Palmgren, F., Querol, X.,
717 Rodriguez, S., Schneider, J., Ten Brink, H., Tunved, P., Tørseth, K., Wehner, B., Weingartner, E., Wiedensohler, A.,
718 Wählin, P.: A European aerosol phenomenology-1: Physical characteristics of particulate matter at kerbside, urban, rural
719 and background sites in Europe, *Atmos. Environ.*, 38, 2561–2577, <https://doi.org/10.1016/j.atmosenv.2004.01.040>, 2004.

720 Viana, M., Amato, F., Alastuey, A., Querol, X., Moreno, T., Dos Santos, S.G., Hecce, M.D., Fernández-Patier, R.: Chemical
721 tracers of particulate emissions from commercial shipping, *Environ. Sci. Technol.*, 43, 7472–7477,
722 <https://doi.org/10.1021/es901558t>, 2009.

723 Vione, D., Maurino, V., Minero, C., Pelizzetti, E.: Phenol photonitration upon UV irradiation of nitrite in aqueous solution II:
724 Effects of pH and TiO₂, *Chemosphere*, 45, 903–910, [https://doi.org/10.1016/S0045-6535\(01\)00036-4](https://doi.org/10.1016/S0045-6535(01)00036-4), 2001.

725 Wang, G., Zhang, R., Gomez, M.E., Yang, L., Zamora, M.L., Hu, M., Lin, Y., Peng, J., Guo, S., Meng, J., Li, J., Cheng, C.,
726 Hu, T., Ren, Y., Wang, Y.Y., Gao, J., Cao, J., An, Z., Zhou, W., Li, G., Wang, J., Tian, P., Marrero-Ortiz, W., Secrest, J.,
727 Du, Z., Zheng, J., Shang, D., Zeng, L., Shao, M., Wang, W., Huang, Y., Wang, Y.Y., Zhu, Y., Li, Y., Hu, J., Pan, B., Cai,
728 L., Cheng, Y., Ji, Y., Zhang, F., Rosenfeld, D., Liss, P.S., Duce, R.A., Kolb, C.E., Molina, M.J., Peng, J., Duan, L., Ji, Y.,
729 Marrero-Ortiz, W., An, Z., Huang, R., Zhang, R., Tie, X., Li, G., Cao, J.: Persistent sulfate formation from London Fog
730 to Chinese haze, *Proc. Natl. Acad. Sci. U. S. A.*, 113, 13630–13635, <https://doi.org/10.1073/pnas.1616540113>, 2016.

731 Worton, D.R., Surratt, J.D., LaFranchi, B.W., Chan, A.W.H., Zhao, Y., Weber, R.J., Park, J.-H., Gilman, J.B., De Gouw, J.,
732 Park, C., Schade, G., Beaver, M.R., St. Clair, J., Crounse, J.D., Wennberg, P., Wolfe, G.M., Harrold, S., Thornton, J.,
733 Farmer, D., Docherty, K.S., Cubison, M., Jimenez, J.L., Frossard, A., Russell, L.M., Kristensen, K., Glasius, M., Mao,
734 J., Ren, X., Brune, B., Browne, E.C., Pusede, S., Cohen, R.C., Seinfeld, J.H., Goldstein, A.H.: Observational insights
735 into high- and low-NO_x aerosol formation from isoprene, *Environ. Sci. Technol.*, 47, 11403–11413,
736 <https://doi.org/10.1021/es4011064>, 2013.

737 Xie, B., Fung, J. C. H., Chan, A., Lau, A.: Evaluation of nonlocal and local planetary boundary layer schemes in the WRF
738 model, *J. Geophys. Res. Atmos.*, 117, D12103, <https://doi.org/10.1029/2011JD017080>, 2012.

739 Xu, L., Guo, H., Boyd, C.M., Klein, M., Bougiatioti, A., Cerully, K.M., Hite, J.R., Isaacman-VanWertz, G., Kreisberg, N.M.,
740 Knote, C., Olson, K., Koss, A., Goldstein, A.H., Hering, S. V., de Gouw, J., Baumann, K., Lee, S.-H., Nenes, A., Weber,
741 R.J., Ng, N.L.: Effects of anthropogenic emissions on aerosol formation from isoprene and monoterpenes in the

742 southeastern United States, *Proc. Natl. Acad. Sci. U. S. A.*, 112, 37–42, <https://doi.org/10.1073/pnas.1417609112>, 2015.

743 Yu, J.Z., Huang, X.-F., Xu, J., Hu, M.: When aerosol sulfate goes up, so does oxalate: Implication for the formation
744 mechanisms of oxalate, *Environ. Sci. Technol.*, 39, 128–133, <https://doi.org/10.1021/es049559f>, 2005.

745 Yu, L., Smith, J., Laskin, A., Anastasio, C., Laskin, J., Zhang, Q.: Chemical characterization of SOA formed from aqueous-
746 phase reactions of phenols with the triplet excited state of carbonyl and hydroxyl radical, *Atmos. Chem. Phys.*, 14,
747 13801–13816, <https://doi.org/10.5194/acp-14-13801-2014>, 2014.

748 Yuan, Z.B., Yu, J.Z., Lau, A.K.H., Louie, P.K.K., Fung, J.C.H.: Application of positive matrix factorization in estimating
749 aerosol secondary organic carbon in Hong Kong and its relationship with secondary sulfate, *Atmos. Chem. Phys.*, 6, 25–
750 34, <https://doi.org/10.5194/acp-6-25-2006>, 2006.

751 Worton, D.R., Surratt, J.D., LaFranchi, B.W., Chan, A.W.H., Zhao, Y., Weber, R.J., Park, J.-H., Gilman, J.B., De Gouw, J.,
752 Park, C., Schade, G., Beaver, M.R., StClair, J., Crouse, J.D., Wennberg, P., Wolfe, G.M., Harrold, S., Thornton, J.,
753 Farmer, D., Docherty, K.S., Cubison, M., Jimenez, J.L., Frossard, A. a, Russell, L.M., Kristensen, K., Glasius, M., Mao,
754 J., Ren, X., Brune, B., Browne, E.C., Pusede, S., Cohen, R.C., Seinfeld, J.H., Goldstein, A.H.: Observational insights
755 into high- and low-NO_x aerosol formation from isoprene, *Environ. Sci. Technol.*, 47, 11403–11413,
756 <https://doi.org/10.1021/es4011064>, 2013.

757 Zhang, H., Yee, L.D., Lee, B.H., Curtis, M.P., Worton, D.R., Isaacman-VanWertz, G., Offenberg, J.H., Lewandowski, M.,
758 Kleindienst, T.E., Beaver, M.R., Holder, A.L., Lonneman, W.A., Docherty, K.S., Jaoui, M., Pye, H.O.T., Hu, W., Day,
759 D.A., Campuzano-Jost, P., Jimenez, J.L., Guo, H., Weber, R.J., De Gouw, J., Koss, A.R., Edgerton, E.S., Brune, W.,
760 Mohr, C., Lopez-Hilfiker, F.D., Lutz, A., Kreisberg, N.M., Spielman, S.R., Hering, S. V., Wilson, K.R., Thornton, J.A.,
761 Goldstein, A.H.: Monoterpenes are the largest source of summertime organic aerosol in the southeastern United States,
762 *Proc. Natl. Acad. Sci. U. S. A.*, 115, 2038–2043, <https://doi.org/10.1073/pnas.1717513115>, 2018.

763 Zhang, Q., Jimenez, J.L., Canagaratna, M.R., Allan, J.D., Coe, H., Ulbrich, I., Alfarra, M.R., Takami, A., Middlebrook, A.M.,
764 Sun, Y.L., Dzepina, K., Dunlea, E., Docherty, K., DeCarlo, P.F., Salcedo, D., Onasch, T., Jayne, J.T., Miyoshi, T.,
765 Shimono, A., Hatakeyama, S., Takegawa, N., Kondo, Y., Schneider, J., Drewnick, F., Borrmann, S., Weimer, S.,
766 Demerjian, K., Williams, P., Bower, K., Bahreini, R., Cottrell, L., Griffin, R.J., Rautiainen, J., Sun, J.Y., Zhang, Y.M.,
767 Worsnop, D.R.: Ubiquity and dominance of oxygenated species in organic aerosols in anthropogenically-influenced
768 Northern Hemisphere midlatitudes, *Geophys. Res. Lett.*, 34, 1–6, <https://doi.org/10.1029/2007GL029979>, 2007.

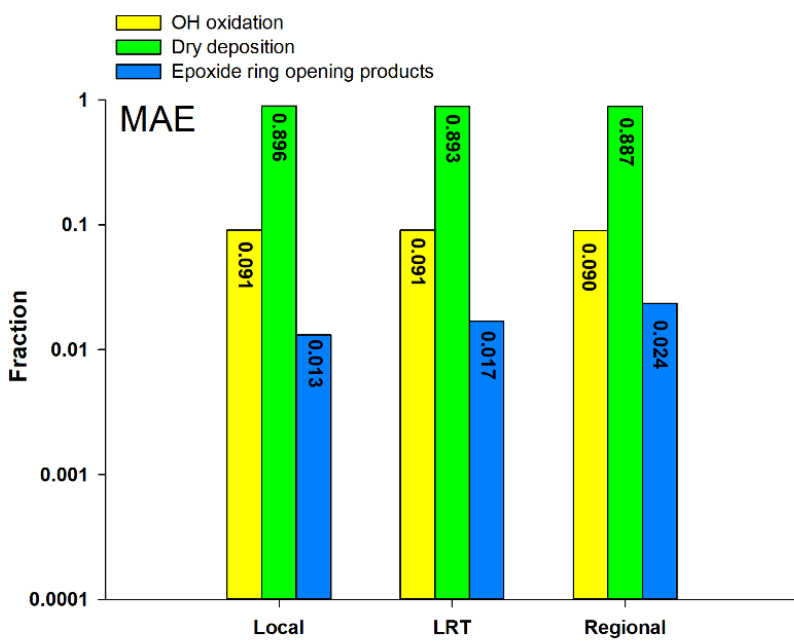
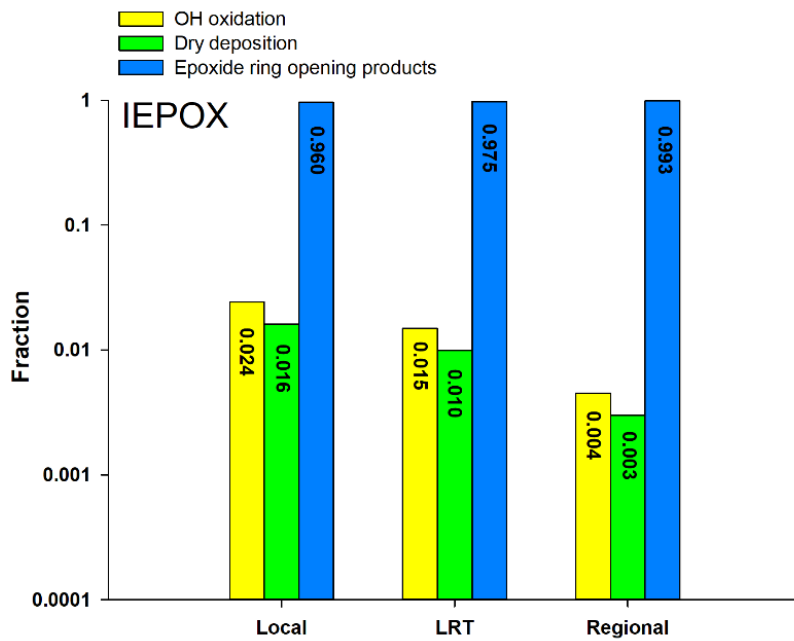
769 Zhang, T., Claeys, M., Cachier, H., Dong, S., Wang, W., Maenhaut, W., Liu, X.: Identification and estimation of the biomass
770 burning contribution to Beijing aerosol using levoglucosan as a molecular marker, *Atmos. Environ.*, 42, 7013–7021,
771 <https://doi.org/10.1016/j.atmosenv.2008.04.050>, 2008.

772 Zhang, Y. X., Shao, M., Zhang, Y.H., Zeng, L.M., He, L.Y., Zhu, B., Wei, Y.J., Zhu, X.L.: Source profiles of particulate organic
773 matters emitted from cereal straw burnings, *J. Environ. Sci.*, 19, 167–175, [https://doi.org/10.1016/S1001-0742\(07\)60027-8](https://doi.org/10.1016/S1001-0742(07)60027-8), 2007.

774

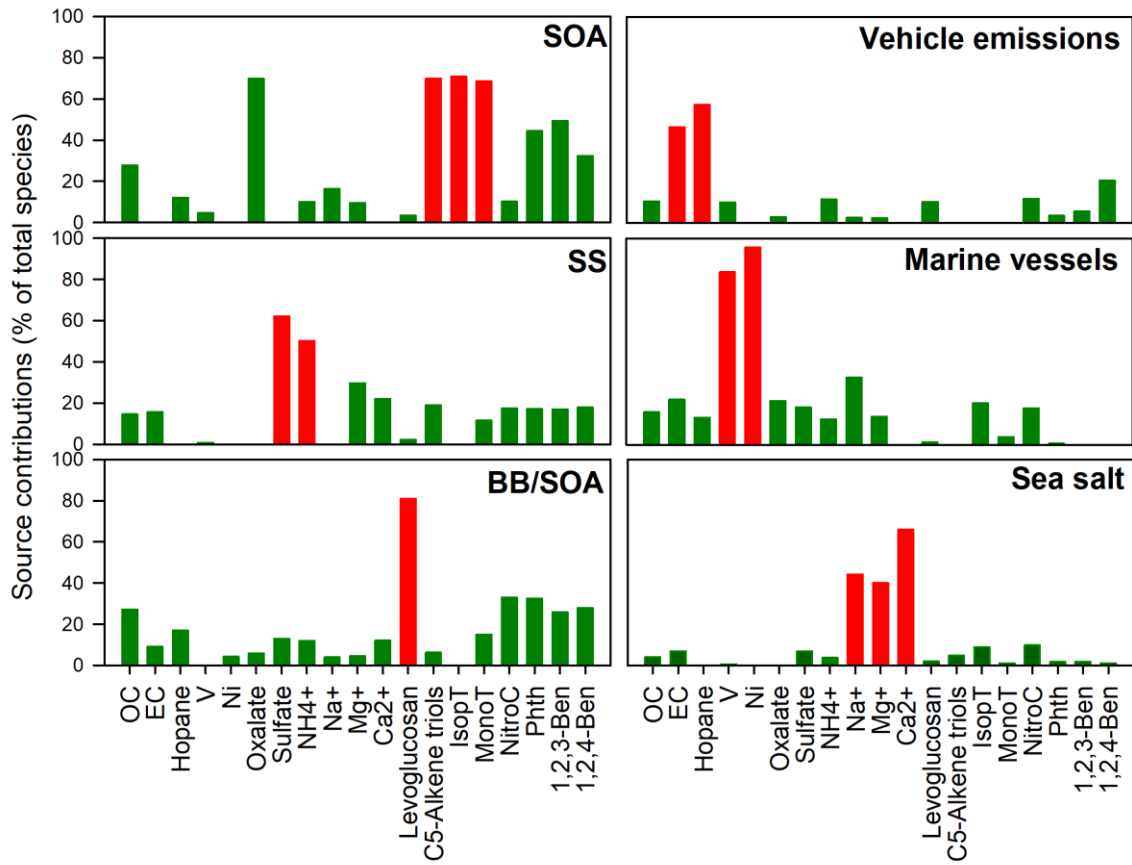
775 Zheng, M., Salmon, L.G., Schauer, J.J., Zeng, L., Kiang, C.S., Zhang, Y., Cass, G.R.: Seasonal trends in PM_{2.5} source
776 contributions in Beijing, China, *Atmos. Environ.*, 39, 3967–3976, <https://doi.org/10.1016/j.atmosenv.2005.03.036>, 2005.

777 Zheng, M., Zhao, X., Cheng, Y., Yan, C., Shi, W., Zhang, X., Weber, R.J., Schauer, J.J., Wang, X., Edgerton, E.S.: Sources of
778 primary and secondary organic aerosol and their diurnal variations, *J. Hazard. Mater.*, 264, 536–544,
779 <https://doi.org/10.1016/j.jhazmat.2013.10.047>, 2014.



780

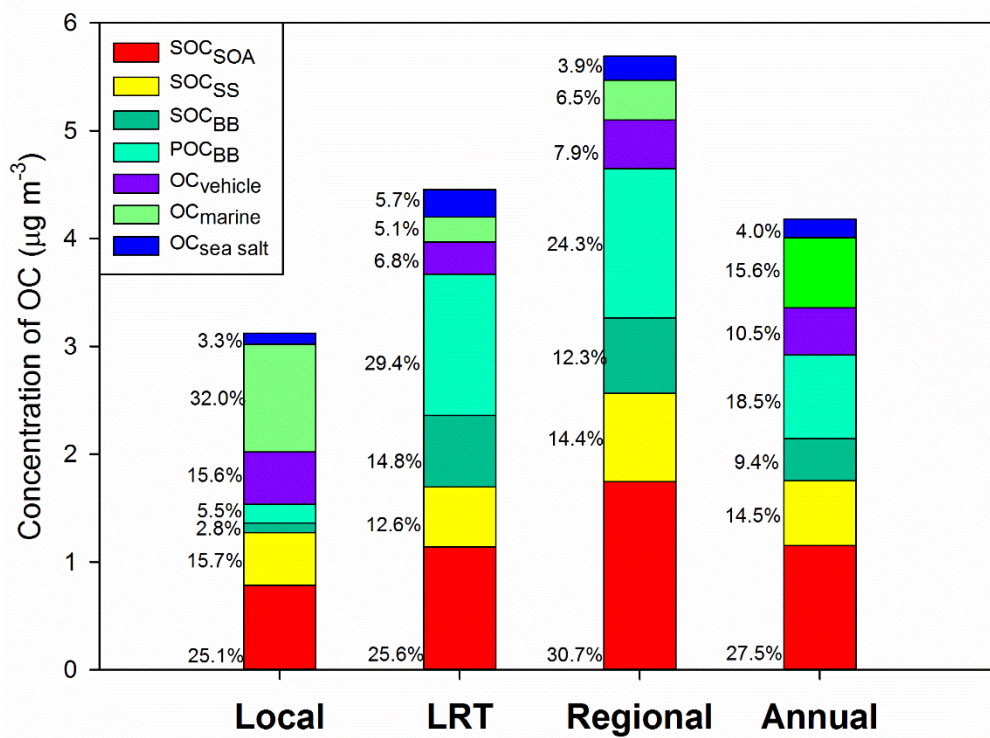
781 Figure 1: Comparison of three degradation processes for IEPOX and MAE under the three synoptic conditions



782

783 Figure 2: PMF-resolved source contributions (% of total species) to ambient PM_{2.5} samples collected in Hong Kong. Red
 784 column: chemical markers for source identification.

785

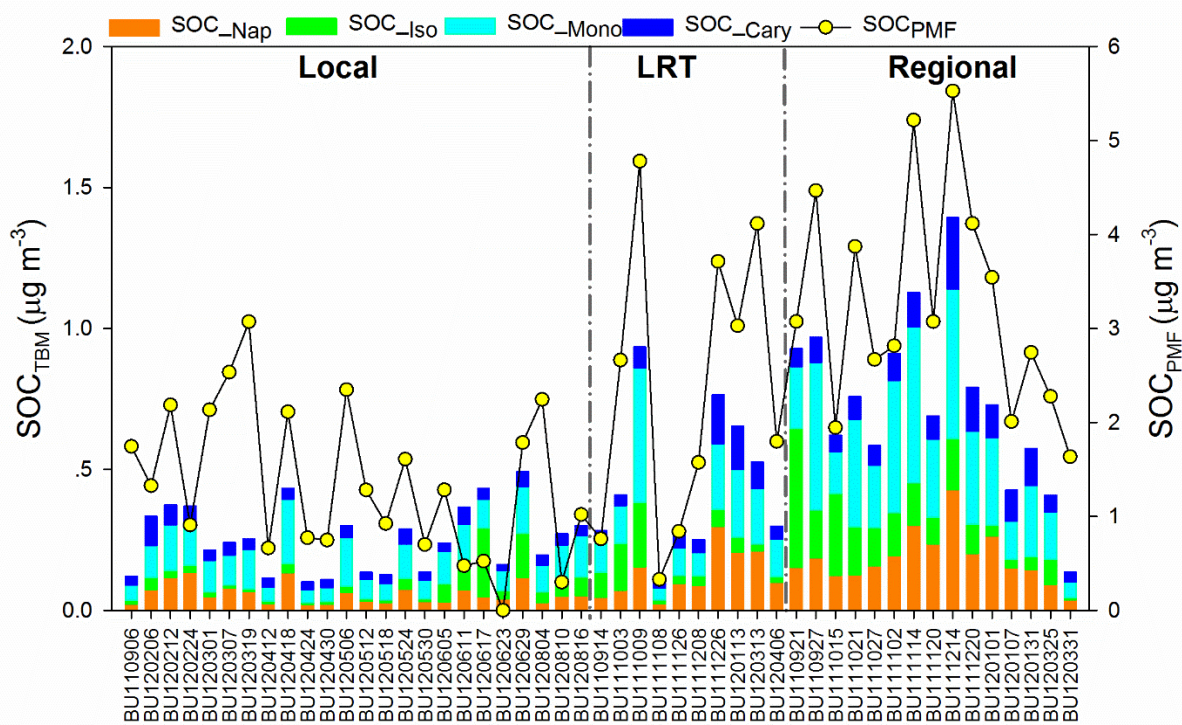


786

787

Figure 3: Source-specific contributions to OC under different meteorological conditions. OC_{BB} was split into POC_{BB} and SOC_{BB}.

788



789

790

Figure 4: Temporal variations of SOC_{PMF} and SOC_{TBM}.

791 Table 1: Concentrations of 14 SOA tracers, 25 polar organic compounds, and nine inorganic ions in PM_{2.5} collected in Hong
 792 Kong under three meteorological conditions.

	Local (N=24)		Long regional transport (N=10)		Regional (N=15)	
	Average	Range	Average	Range	Average	Range
<i>Tracers for isoprene SOA (ng m⁻³)</i>						
2-Methylglyceric acid	0.56±0.31	0.22-1.42	1.28±0.86	0.29-2.61	2.36±1.75	0.02-6.42
2-Methylthreitol	2.34±3.95	0.33-18.79	2.88±2.97	0.57-9.60	6.23±5.69	0.35-23.37
2-Methylerythritol	7.06±13.95	0.54-64.67	6.94±7.81	1.08-23.58	13.49±12.23	0.48-47.62
cis-2-Methyl-1,3,4-trihydroxy-1-butene	0.87±1.25	0.15-6.06	2.00±2.56	0.33-8.62	5.78±4.57	0.22-17.19
3-Methyl-2,3,4-trihydroxy-1-butene	0.52±0.49	0.15-2.00	1.03±1.17	0.23-4.08	2.40±1.91	0.18-7.31
trans-2-Methyl-1,3,4-trihydroxy-1-butene	1.28±1.25	0.15-5.08	5.25±5.59	0.48-18.68	10.52±8.19	0.37-25.23
3-MeTHF-3,4-diols	0.18±0.06	0.15-0.34	0.21±0.07	0.15-0.32	0.29±0.12	0.15-0.60
∑C ₅ -alkene triols	2.68±2.52	0.45-8.89	8.27±8.92	1.20-31.37	18.71±13.14	0.78-40.08
∑Isoprene tracers (exclude triols)	10.06±18.09	1.22-84.87	11.23±11.18	1.93-35.70	22.32±18.94	1.17-77.09
∑Isoprene tracers	12.74±20.13	1.67-93.41	19.51±19.41	3.14-67.07	41.03±29.71	1.95-117.17
<i>Tracers for monoterpenes SOA (ng m⁻³)</i>						
3-Hydroxyglutaric acid	3.40±2.09	0.72-9.14	6.11±5.42	0.66-19.15	11.53±6.27	1.35-22.04
3-Hydroxy-4,4-dimethylglutaric acid	0.53±0.12	0.42-0.93	0.71±0.30	0.43-1.39	0.91±0.28	0.41-1.39
3-Methyl-1,2,3-butanetricarboxylic acid	0.59±0.19	0.40-1.18	0.84±0.39	0.45-1.76	1.28±0.52	0.42-2.14
3-Isopropylpentanedioic acid	1.07±0.38	0.55-1.85	1.52±0.86	0.51-3.46	2.57±1.52	0.61-4.86
3-Acetyl pentanedioic acid	0.82±0.23	0.45-1.19	1.13±0.55	0.49-2.42	1.71±0.87	0.54-3.20
∑ Monoterpenes tracers	6.41±2.75	2.63-13.49	10.31±7.33	2.54-28.17	18.00±9.28	3.33-32.57
<i>Tracers for β-caryophyllene SOA (ng m⁻³)</i>						
β-Caryophyllinic acid	0.94±0.41	0.49-2.36	1.73±1.16	0.75-3.99	2.33±1.21	0.80-5.82
<i>Tracers for Naphthalene SOA (ng m⁻³)</i>						
Phthalic acid	2.26±1.38	0.80-5.17	4.97±3.30	0.92-11.41	7.16±3.61	1.41-16.42
<i>Dicarboxylic acids (ng m⁻³)</i>						
Succinic acid	2.10±1.63	0.65-6.23	4.56±4.80	0.80-14.18	5.27±3.43	0.68-12.19
Maleic acid	0.42±0.27	0.14-1.47	0.42±0.23	0.14-0.84	0.36±0.18	0.15-0.78
Malic acid	2.67±1.49	0.64-5.59	4.20±3.74	0.60-13.12	8.10±4.12	1.33-13.86
Glutaric acid	2.63±6.06	0.82-30.89	2.36±1.73	0.79-4.99	2.85±1.53	0.67-6.05
Citramalic acid	0.76±0.23	0.38-1.30	0.86±0.32	0.38-1.48	1.23±0.47	0.52-2.00
Terephthalic acid	9.28±7.49	2.16-31.86	30.21±27.20	3.58-79.61	36.89±23.84	3.77-79.25
Adipic acid	1.34±1.42	0.54-6.20	1.20±0.46	0.64-2.21	1.48±0.66	0.67-3.08
Pimelic acid	0.68±0.10	0.51-0.93	0.82±0.29	0.52-1.47	0.99±0.35	0.52-1.94
Oxalic acid (μg m ⁻³)	0.35±0.20	0.11-0.86	0.38±0.23	0.09-0.72	0.54±0.21	0.29-0.94
<i>Saccharides (ng m⁻³)</i>						
Levoglucosan	22.51±41.16	0.64-161.16	120.79±129.55	3.21-362.74	128.52±140.39	8.64-474.15
Meso-erythritol	0.11±0.10	0.03-0.43	0.29±0.25	0.03-0.74	0.44±0.28	0.07-1.22
Xylitol	0.29±0.11	0.21-0.69	0.50±0.28	0.23-1.02	0.52±0.22	0.22-1.03
Xylose	1.24±1.08	0.50-4.57	4.65±4.45	0.58-13.34	5.34±4.31	0.81-16.12
Galactose	1.82±2.02	0.37-9.97	3.31±1.97	1.09-7.08	3.51±1.71	1.02-6.84
Mannitol	0.16±0.04	0.12-0.26	0.21±0.07	0.13-0.37	0.23±0.07	0.13-0.37
Fructose	2.30±3.19	0.26-15.58	3.64±3.89	0.38-13.41	4.32±2.54	1.65-9.32
Galactosan	1.09±0.53	0.79-2.99	2.58±2.47	0.84-7.20	2.68±2.40	0.88-7.99
Sorbitol	1.45±0.37	1.14-2.54	1.55±0.28	1.21-1.96	1.70±0.40	1.31-2.62
Glucose	1.55±0.89	0.50-3.83	1.20±0.61	0.40-2.07	1.51±0.92	0.52-3.29
Sucrose	0.94±1.81	0.42-9.43	0.58±0.14	0.42-0.91	0.57±0.08	0.45-0.76
Arbitol	0.25±0.10	0.00-0.57	0.40±0.20	0.22-0.78	0.42±0.17	0.22-0.85
<i>Other compounds (ng m⁻³)</i>						

4-Nitrocatechol	0.90±0.12	0.78-1.35	1.30±0.62	0.84-2.75	1.55±0.83	0.85-4.00
Cholesterol	1.29±0.25	0.94-1.81	1.30±0.28	1.01-1.93	1.20±0.27	0.95-1.89
1,2,3-Benzenetricarboxylic Acid	1.23±0.67	0.47-2.46	2.25±1.34	0.63-4.70	3.97±2.54	0.54-9.50
1,2,4-Benzenetricarboxylic Acid	1.77±1.28	0.47-6.17	3.32±2.34	0.88-6.77	5.16±3.30	0.73-12.54
<i>Major ion ($\mu\text{g m}^{-3}$)</i>						
Sulfate	11.43±5.98	3.28-30.32	13.02±9.25	1.49-29.25	17.35±5.20	8.90-29.29
Nitrate	0.89±1.17	0.05-3.39	1.62±2.10	0.08-5.84	1.41±1.51	0.38-5.49
Chloride	0.18±0.17	0.06-0.77	0.17±0.15	0.07-0.45	0.14±0.09	0.07-0.40
Ammonia	2.05±0.91	0.47-4.12	2.26±1.48	0.30-4.36	2.99±0.72	1.82-4.69
Potassium	0.11±0.07	0.03-0.36	0.29±0.17	0.05-0.49	0.40±0.22	0.15-0.94
Magnesium	0.01±0.01	0.00-0.03	0.02±0.01	0.00-0.04	0.02±0.01	0.00-0.04
Calcium	0.03±0.03	0.00-0.13	0.08±0.07	0.02-0.23	0.08±0.04	0.02-0.15
Sodium	0.09±0.09	0.01-0.40	0.16±0.14	0.03-0.52	0.14±0.06	0.08-0.30

Table 2: PMF and TBM-resolved OCs, concentrations of gas pollutants, PM_{2.5}, EC, OC, and major aerosol characteristics under different meteorological conditions.

	Local (N=24)		Long regional transport (N=10)		Regional (N=15)		Annual (N=49)	
	Average	Range	Average	Range	Average	Range	Average	Range
PM _{2.5} (µg m ⁻³)	24.11±9.99	10.04-49.28	32.23±14.81	7.63-50.68	38.5±10.48	26.20-65.28	30.17±12.72	7.63-65.28
EC (µgC m ⁻³)	1.02±0.57	0.47-2.75	0.85±0.60	0.14-2.10	1.14±0.45	0.50-2.12	1.02±0.54	0.14-2.75
OC _{measured}	2.94±1.11	1.61-5.75	4.16±2.53	1.25-8.53	6.15±2.51	3.21-12.97	4.18±2.37	1.25-12.97
	<i>PMF apportioned OC (µgC m⁻³)</i>							
SOC _{SOA}	0.78±0.65	0.00-2.27	1.14±0.82	0.18-2.72	1.75±0.75	0.65-3.29	1.15±0.82	0.00-3.29
SOC _{SS}	0.49±0.37	0.00-1.74	0.56±0.67	0.00-1.81	0.82±0.38	0.24-1.65	0.60±0.46	0.00-1.81
OC _{BB} (POC _{BB} +SOC _{BB})	0.26±0.63	0.00-2.34	1.97±2.26	0.00-6.34	2.08±2.63	0.00-8.96	1.17±1.99	0.00-8.96
OC _{Vehicle}	0.49±0.46	0.00-2.07	0.30±0.42	0.00-1.26	0.45±0.36	0.01-1.26	0.44±0.42	0.00-2.07
OC _{Marine}	1.00±0.63	0.04-2.97	0.23±0.19	0.00-0.51	0.37±0.21	0.08-0.71	0.65±0.18	0.00-2.97
OC _{Sea salt}	0.10±0.11	0.00-0.53	0.25±0.33	0.00-1.13	0.22±0.16	0.00-0.62	0.17±0.19	0.00-1.13
SOC _{BB}	0.09±0.21	0.00-0.79	0.66±0.76	0.00-2.13	0.70±0.88	0.00-3.01	0.39±0.67	0.00-3.01
SOC _{PMF}	1.36±0.81	0.00-3.07	2.36±1.54	0.33-4.78	3.27±1.18	1.63-5.53	2.15±1.37	0.00-5.53
SOC _{PMF} /OC (%)	43.0±16.8%	0.0%-66.5%	52.3±21.1%	30.0%-85.3%	60.2±13.7%	36.2%-78.8%	50.2±18.2%	0.0%-85.3%
	<i>Tracer based method estimated OC (µgC m⁻³)</i>							
SOC _{Iso}	0.04±0.06	0.01-0.24	0.07±0.07	0.01-0.23	0.14±0.12	0.01-0.49	0.08±0.09	0.01-0.49
SOC _{Mono}	0.14±0.06	0.06-0.29	0.22±0.16	0.05-0.60	0.38±0.20	0.07-0.69	0.23±0.17	0.05-0.69
SOC _{Cary}	0.04±0.02	0.02-0.10	0.08±0.05	0.03-0.17	0.10±0.05	0.03-0.25	0.07±0.05	0.02-0.25
SOC _{Nap}	0.06±0.04	0.02-0.13	0.13±0.09	0.02-0.30	0.19±0.09	0.04-0.43	0.11±0.09	0.02-0.43
SOC _{TBM}	0.28±0.13	0.11-0.53	0.50±0.29	0.12-1.06	0.81±0.35	0.15-1.53	0.49±0.34	0.11-1.53
SOC _{TBM} /OC	10.2±5.1%	3.8%-22.7%	13.0±4.6%	5.3%-20.7%	13.4±4.3%	4.7%-19.6%	11.8±4.9%	3.8%-22.7%
	<i>Gas Pollutants and other aerosol characteristics</i>							
O _{3_} average (ppb)	11.61±7.3	2.93-32.12	13.96±7.94	2.86-26.92	20.64±8.74	2.88-31.84	14.85±8.69	2.86-32.12
NO _{2_} average (ppb)	34.56±10.66	16.7-54.32	34.59±7.62	21.74-42.85	42.98±7.10	32.72-60.37	37.15±9.76	16.70-60.37
SO _{2_} average (µg m ⁻³)	4.14±2.92	0.7-10.38	3.81±1.88	2.23-7.30	5.38±2.24	2.96-10.45	4.45±2.57	0.70-10.45
O _x (µg m ⁻³)	87.45±26.26	49.72-138.49	93.18±21.37	61.66-125.79	122.39±17.70	69.54-145.90	99.31±27.42	49.72-145.90
p[NO ₃] (ppb h ⁻¹)	1.25±0.96	0.30-4.17	1.36±0.94	0.31-3.29	2.45±1.02	0.23-3.76	1.64±1.10	0.23-4.17
NO _{3_} average (ppb)	0.05±0.04	0.01-0.18	0.06±0.04	0.01-0.14	0.10±0.04	0.01-0.16	0.07±0.05	0.01-0.18
H _p ⁺ (M)	1.72±1.04	0.02-3.78	2.66±1.50	0.49-5.43	3.22±0.79	2.31-4.76	2.37±1.25	0.02-5.43
pH	(-0.20)±0.52	(-0.58)-1.81	(-0.31)±0.32	(-0.74)-0.31	(-0.50)±0.10	(-0.68)-(-0.36)	(-0.28)±0.42	(-0.74)-1.81
LWC (µg m ⁻³)	66.64±46.51	2.68-184.71	42.88±28.80	6.60-86.03	51.65±17.69	30.51-101.12	57.2±37.15	2.68-184.71

797 Table 3: Regression analysis (Pearson's R) of PMF and TBM-resolved SOCs, SO₂, NO₂, O₃, tropospheric odd oxygen (O_x),
 798 particle acidity (H_p⁺), total particle-phase licate water content (LWC_P), and sulfate **: P<0.01; *: P<0.05. Note: R>0.5 are
 799 bold.

	Pearson's R								
	SOC_Iso	SOC_Mono	SOC_Cary	SOC_Nap	SOC _{TBM}	SOC _{BB}	SOC _{SOA}	SOC _{SS}	SOC _{PMF}
O ₃ (ppb)	0.374**	.401**	0.011	0.246	.374**	-0.111	.502**	.557**	.434**
NO ₂ (ppb)	.064	.516**	.586**	.528**	.500**	.469**	.570**	0.165	.627**
SO ₂ (ppb)	0.044	0.198	.463**	.296*	0.255	.357*	0.035	-0.052	0.179
O _x (μg m ⁻³)	0.257	.600**	.433**	.535**	.577**	0.281	.707**	.445**	.711**
NO ₃ (ppb)	.413**	.530**	0.101	.313*	.480**	-0.077	.637**	.574**	.538**
Sulfate (μg m ⁻³)	.287*	.610**	.405**	.506**	.579**	0.23	.646**	.886**	.799**
H _p ⁺ (M)	0.249	.334*	.391**	.388**	.395**	.400**	0.164	0.24	.376**
LWC _P (μg m ⁻³)	-0.18	0.18	0.115	0.209	0.113	0.003	.413**	.438**	.397**

800

801 Table 4: Results of multivariate linear analysis of PMF and TBM-resolved SOCs, NO₂, NO₃, sulfate, particle acidity (H_p⁺),
 802 and total particle-phase licate water content (LWC_P). **: P<0.01; *: P<0.05. Note: significant regressions are bold.

	normalized β-coefficient								
	SOC_Iso	SOC_Mono	SOC_Cary	SOC_Nap	SOC _{TBM}	SOC _{BB}	SOC _{SOA}	SOC _{SS}	SOC _{PMF}
NO ₂ (ppb)	-0.013	0.351**	0.660**	0.445**	0.383**	0.639**	0.270*	-0.303**	0.373**
NO ₃ (ppb)	0.309	0.174	-0.382**	-0.077	0.101	-0.509**	0.384**	0.234**	0.059
Sulfate (μg m ⁻³)	0.343	0.417*	0.240	0.202	0.393*	0.083	0.303	0.913**	0.530**
H _p ⁺ (M)	-0.138	0.047	0.378*	0.348*	0.129	0.503**	-0.053	-0.189*	0.151
LWC _P (μg m ⁻³)	-0.392	-0.135	-0.091	0.071	-0.171	-0.073	0.125	0.096	0.071

803